TECHNICAL UNIVERSITY OF LIBEREC
Faculty of Mechanical Engineering

Modelling of the cavitation bubbles dynamics

Master Thesis

Study programme:	N2301 Mechanical Engineering
Study branch:	Machines and Equipment Design
Author:	**Merim Elezović**
Thesis Supervisors:	Ing. Miloš Müller, Ph.D. Department of Power Engineering Equipment

Liberec 2021

TECHNICAL UNIVERSITY OF LIBEREC
Faculty of Mechanical Engineering

Master Thesis Assignment Form

Modelling of the cavitation bubbles dynamics

Name and surname: **Merim Elezović**
Identification number: S19000342
Study programme: N2301 Mechanical Engineering
Study branch: Machines and Equipment Design
Assigning department: Department of Power Engineering Equipment
Academic year: **2020/2021**

Rules for Elaboration:

Elaboration of a review on the models used for the cavitation dynamics description
Preparation of a numerical model for the simulation of the cavitation dynamic based on the Rayleigh-Plesset equation
Validation of the numerical model towards available experiments
Testing the influence of the liquid properties and boundary conditions on the cavitation bubble dynamics using the numerical model
Investigation of a possibility of the numerical model to predict the cavitation erosion

Scope of Graphic Work: 10
Scope of Report: 50
Thesis Form: printed/electronic
Thesis Language: English

List of Specialised Literature:

FRANC, Jean-Pierre a Jean-Marie MICHEL. *Fundamentals of cavitation*. Dordrecht: Kluwer Academic Publishers, [2004]. Fluid mechanics and its applications, volume 76. ISBN 1-4020-2232-8.
BRENNEN, Christopher E. *Cavitation and bubble dynamics*. New York: Cambridge University Press, 2014. ISBN 9781107644762.

Thesis Supervisors: Ing. Miloš Müller, Ph.D.
Department of Power Engineering Equipment

Date of Thesis Assignment: November 1, 2020
Date of Thesis Submission: April 30, 2022

L.S.

prof. Dr. Ing. Petr Lenfeld
Dean

doc. Ing. Petra Dančová, Ph.D.
Head of Department

Liberec November 1, 2020

Declaration

I hereby certify, I, myself, have written my master thesis as an original and primary work using the literature listed below and consulting it with my thesis supervisor and my thesis counsellor.

I acknowledge that my bachelor master thesis is fully governed by Act No. 121/2000 Coll., the Copyright Act, in particular Article 60 – School Work.

I acknowledge that the Technical University of Liberec does not infringe my copyrights by using my master thesis for internal purposes of the Technical University of Liberec.

I am aware of my obligation to inform the Technical University of Liberec on having used or granted license to use the results of my master thesis; in such a case the Technical University of Liberec may require reimbursement of the costs incurred for creating the result up to their actual amount.

At the same time, I honestly declare that the text of the printed version of my master thesis is identical with the text of the electronic version uploaded into the IS/STAG.

I acknowledge that the Technical University of Liberec will make my master thesis public in accordance with paragraph 47b of Act No. 111/1998 Coll., on Higher Education Institutions and on Amendment to Other Acts (the Higher Education Act), as amended.

I am aware of the consequences which may under the Higher Education Act result from a breach of this declaration.

June 4, 2021 Merim Elezović

ACKNOWLEDGEMENTS

I wish to show my deepest gratitude to my thesis supervisor, Ing. Miloš Müller, Ph.D., who introduced me to the cavitation phenomenon, and provided me with all the guidance I needed while working on this study. I wish to acknowledge the love and support of my girlfriend Amila who managed to come up with patience and answers even in the most difficult moments that this journey brought. I am grateful to my parents and my sister for believing in me and supporting me unconditionally.

Finally, I would like to thank the Government of the Czech Republic, and the Ministry of Education, Youth and Sports for giving me the opportunity and funds to study in Czech Republic and take a huge leap forward in my life.

ABSTRACT

The goal of this study is to apply a numerical model for cavitation bubble dynamics that is based on the existing Rayleigh-Plesset equation (RPE). Physical background and derivation of the RPE are given, as well as the basic phenomena associated with cavitation, such as nucleation, shockwaves, and microjets. Several adverse effects of cavitation are discussed, in addition to domains in which cavitation was found to be useful, and the classification of cavitation. Since RPE is a second order ordinary differential equation (ODE), it had to be converted into a system of two first order ODEs before being solved numerically. Runge-Kutta numerical method of fourth order was selected as the most suitable method for solving a system of ODEs, and then applied on the relations in the RPE. For the model application, computational power of Microsoft Excel was determined to be sufficient to handle all the necessary calculations. Furthermore, the impact of changes in different criteria, initial conditions and fluid parameters is studied, such as: bubble initial radius, pressure amplitude, surface tension, and liquid viscosity. Model is then verified based on existing numerical results. Model is then validated towards two types of experiments – laser-induced cavitation bubble, and spark-generated bubble. Finally, applicability of the model for cavitation erosion prediction is briefly discussed.

Keywords: cavitation, bubble dynamics, Rayleigh-Plesset equation, laser-induced bubble, spark-generated bubble.

TABLE OF CONTENTS

TABLE OF FIGURES

NOMENCLATURE

List of symbols

Roman letters

SYMBOL	DESCRIPTION	UNIT
C	Coefficient of pressure	[-]
c	Speed of sound	[m/s]
d	Diameter	[m]
E	Energy	[J]
f	Frequency	[Hz]
H	Enthalpy	[J]
k	Polytropic coefficient	[-]
l	Characteristic dimension of a body	[m]
p	Pressure	[Pa]
R	Bubble radius	[m]
r	Radial coordinate	[m]
S	Surface tension	[N/m^2]
T	Temperature	[K]
t	Time	[s]
u	Velocity	[m/s]

Greek letters

γ	Ratio of distance to the wall and maximum bubble radius	[-]
κ	Ratio of specific heats	[-]
μ	Dynamic viscosity	[Pa·s]
ν	Kinematic viscosity	[m^2/s]
ρ	Fluid density	[kg/m^3]
σ	Cavitation number	[-]
τ_{La}	Full width at half maximum of the laser power	[s]
φ	Increment function	[-]
ω	Bubble frequency	[Hz]

Subscripts

B	Bubble
c	Critical
col	Collapse
E	Equilibrium
g	Gas
i	Incipient
L	Liquid
La	Laser
m	Maximum
N	Natural
R	Value at the bubble wall
Ra	Rayleigh
v	Vapour
0	Initial
∞	Far in the liquid

List of abbreviations

CCD	Charge-coupled device
DC	Direct current
LED	Light-emitting diode
LIB	Laser-induced breakdown
ND:Yag	Neodymium-doped Yttrium Aluminium Garnet
ODE	Ordinary differential equation
PVDF	Polyvinylidene fluoride
RK	Runge-Kutta
RPE	Rayleigh-Plesset equation

1 INTRODUCTION

In order to describe cavitation properly, it is necessary to start by discussing the process of nucleation. Nucleation is caused by weaknesses that cause lowering the achievable tension inside a fluid [1]. If temporary, microscopic voids arise within the fluid due to random thermal motions of the molecules, and they can form the nuclei required for rupture and growth to macroscopic bubbles. This is named homogeneous nucleation and the corresponding maximum tension can be predicted by kinetic theory. On the other hand, more common situation is the occurence of major weaknesses at the boundary between the liquid and the solid wall of the container, or between the liquid and small particles suspended in the liquid. In that case, nucleation is termed as heterogeneous nucleation. Formation of micron-sized bubbles (microbubbles) of contaminant gas represents another form of weakness which can be found in crevices within the solid boundary or within suspended particles. Finally, fourth important form of contamination is cosmic radiation, during which nucleation is initiated due to a collision between a high energy particle and a molecule of the liquid [2].

Cavitation could be described from another perspective by comparing it to boiling process. Boiling is a process where the state of a liquid is changed by heating process under constant pressure. Cavitation, on the other hand, represents depressurisation at a (relatively) constant temperature, as seen in the Figure 1.1. Main difference is that change of temperature usually occurs at a boundary of a liquid, whereas pressure change can occur uniformly throughout liquid body, thus inducing cavitation in that body.

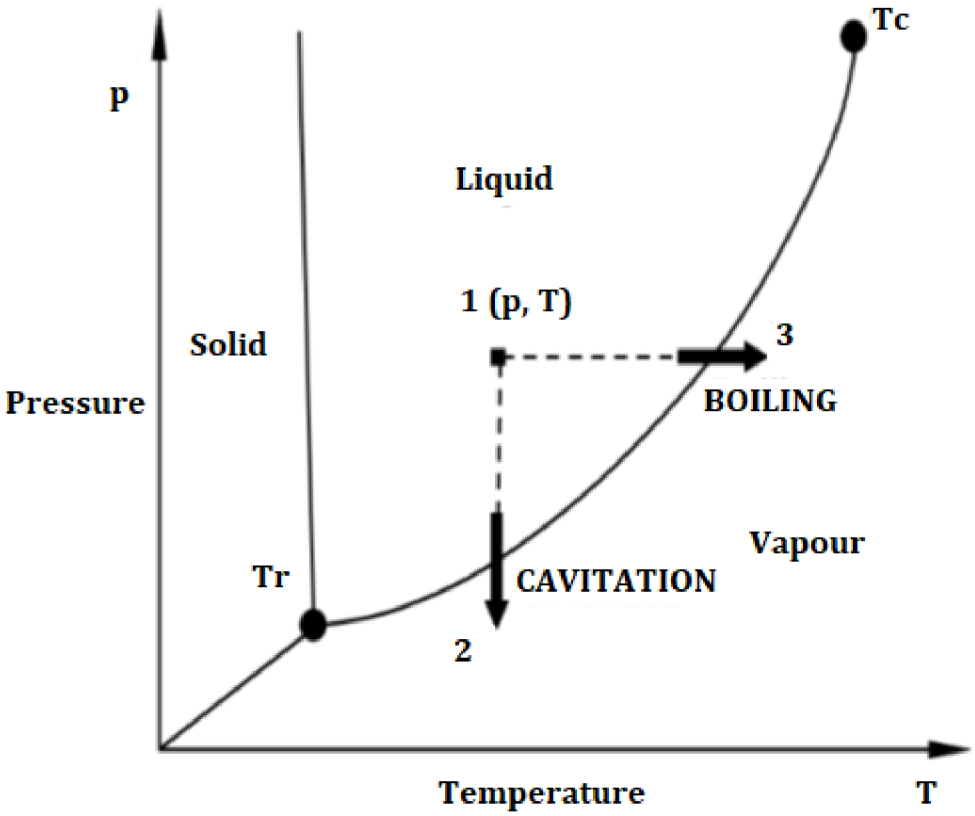

Figure 1.1 Pressure-temperature phase diagram (e.g. water) [27]

Some of the typical locations and situations where cavitation may occur are:

- Venturi nozzles [3] (restriction in the cross sectional area of a duct) and upper sides of blades in pumps and propellers (curvature of flow streamlines due to local geometry) – local increase of velocity and pressure drop.
- Jets and wakes – fluctuations of turbulent pressure.
- Dam spillways – local roughness of the wall.
- Water hammer – strong fluid acceleration and pressure drop.

The most important consequences of cavitation are:

- material erosion - Figure 1.2 [4],
- vibrations and noise,
- numerous adverse effects on the performance of the system, such as the efficiency of turbomachinery [5], energy dissipation, increase in drag and reduction in lift of a foil, etc.).

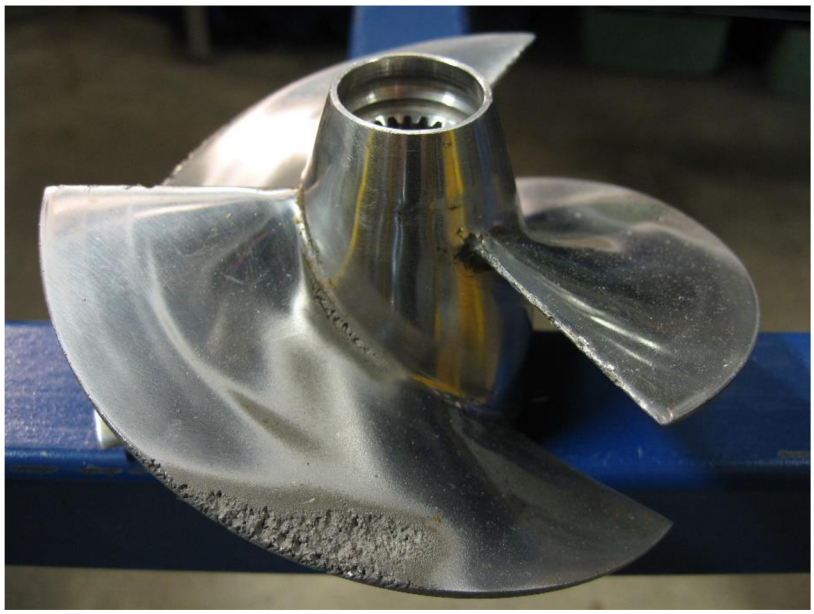

Figure 1.2 Cavitation propeller damage [26]

Despite these adverse effects, cavitation found use in some positive applications as well, some of which are:

- particle dispersion in a liquid,
- surface cleaning by cavitating jets,
- massage and bacteria destruction in medicine.

Cavitation could be classified according to the content of the bubble, and according to the mode of bubble generation. A bubble could contain gas or vapour, or a mixture of both. According to the mode of bubble generation, the classification is as follows:

- Hydrodynamic cavitation – a bubble is generated when a liquid flows through a region of low pressure (accelerated flow), which is lower than vapourisation pressure.
- Acoustic cavitation – strong acoustic field is applied to a stationary system, causing ruptures in the liquid and formation of cavities (bubbles).
- Optical cavitation – or laser-induced cavitation occurs when high intensity light generated by a laser is focused into fluid, and the pulse causes ruptures in the fluid.
- Particle cavitation – bubble growth occurs in a superheated fluid, growing from microscopic bubbles to macroscopic ones [6].

Important parameter for describing cavitation in a flowing system is cavitation number σ which represents how close the pressure of a flowing liquid is to the vapour pressure of that liquid [2]. Ultimately, it describes the possibility for cavitation, and it is defined as:

$$\sigma = 2\frac{p_\infty - p_v}{\rho_L u_\infty^2} \tag{1.1}$$

where p_∞ and u_∞ are a reference pressure and velocity, respectively, ρ_L is the liquid density and p_V is the saturated vapour pressure as a function of reference temperature T_∞. If σ is high enough, single phase flow will occur. Incipient cavitation number σ_i is the cavitation number at which the cavitation is first observed to occur. Number of vapour bubbles will increase as σ is reduced. For a flow of liquid that cannot withstand any tension and in which vapour bubbles appear when the liquid pressure reaches vapour pressure, it follows that:

$$\sigma_i = -C_{pmin} \tag{1.2}$$

where C_{pmin} is the minimum value of the coefficient of pressure, and the incipient number could be obtained from measurements of the single-phase flow. However, numerous factors can cause the actual values of σ_i to be different than -C_{pmin}.

Once initial formation of bubbles is described, it can be proceeded to setting up governing equations describing the dynamics of bubble growth and collapse. Numerous researchers were intrigued by the dynamics of a cavitation bubble, but the one who gets the most recognition for being the first one to build a mathematical model describing bubble dynamics is Lord Rayleigh [7]. The bubble dynamics will be governed by the Rayleigh-Plesset equation (RPE), found in e.g. Franc & Michel [8], which connects the instantaneous bubble radius, $R(t)$, to the pressure p_∞, far from the bubble. The equation is given as:

$$\frac{p_B(t) - p_\infty(t)}{\rho_L} = R\frac{d^2R}{dt^2} + \frac{3}{2}\left(\frac{dR}{dt}\right)^2 + \frac{4\nu_L}{R}\frac{dR}{dt} + \frac{2S}{\rho_L R} \tag{1.3}$$

where ν_L is the kinematic viscosity of the liquid and S is the surface tension. Derivation of equation 1.3 is given in detail in subsection 2.1. It is also necessary to define an estimate of the maximum radius to which a cavitation bubble develops

during its flow through a region of pressure below the vapour pressure. The growth of a bubble is roughly given by:

$$\frac{dR}{dt} = u_\infty\left(-\sigma - C_{pmin}\right)^{\frac{1}{2}} \tag{1.4}$$

and the estimate of maximum radius of the bubble, R_m is:

$$R_m \approx 2l(-\sigma - C_{pmin}) \tag{1.5}$$

where l is the characteristic dimension of a body around which the external flow occurs.

Previous discussion is valid under the assumption that there were no major temperature differences generated in the liquid during growth, which is the case in only some liquids (e.g. water) at lower temperatures. If temperature differences arise between the liquid and the vapour/liquid interface, it will slow down the growth rate. This is termed the thermal effect [9] and it reduces harmful effects of cavitation.

It is possible to derive an expression for the natural frequency of the bubble by one derivation of the Rayleigh-Plesset equation. It is shown that bubble has a natural frequency ω_N, given by:

$$\omega_N = \left[\frac{1}{\rho_L R_E^2}\left\{3k(\bar{p}_\infty - p_V) + 2(3k-1)\frac{S}{R_E}\right\}\right]^{\frac{1}{2}} \tag{1.6}$$

where R_E is the mean or equilibrium radius of the bubble, $(\bar{p}_\infty - p_V)$ is the mean liquid pressure minus vapour pressure and k is a polytropic index for the non-condensable gas in the bubble. Bubbles in the range of 10 μm to 100 μm have natural frequencies in the range 10 to 100 kHz.

Bubble collapse is a very important topic mainly because of the noise and material damage that can be caused by the high pressures, temperatures and velocities that may result from the collapse itself. The collapse begins at the maximum bubble radius R_m, with a partial pressure of gas, p_{gm}. Maximum bubble pressure generated during the first collapse could be about 10^{10} bar and the maximum temperature could be 4×10^4 times the ambient temperature. However, certain factors such as the

effect of compressibility reduce these values. As long as there is some non-condensable gas in the bubble to slow down the collapse, the significance of compressibility is its role in the formation of shock waves during the rebounding phase after the collapse. The temperatures and pressures predicted to occur in the gas are extremely high.

While previous analysis assumed spherical symmetry, it is sometimes necessary to analyse cases when the bubble surroundings are asymmetrical. In case when there is a nearby solid boundary, a re-entrant microjet can be formed and it is directed toward the solid boundary [10]. Another possibility is a bubble collapsing in the proximity of a free surface, when a re-entrant microjet is directed away from the surface. In order to direct the microjet away from the surface, it is possible to apply flexible coatings or liners and thus prevent cavitation damage. Third asymmetry can be closeness of other bubbles in a form of a finite cloud of bubbles, when the jets will develop and be directed toward the center of the cloud.

Since bubble collapse is a process that produces localised shock waves and microjets, it can be expected that there will be surface stresses in case the collapse occurs in its proximity. With softer material, single bubble collapse causes individual pits to appear, whereas with the harder materials the repetition of the loading causes local surface fatigue failure and thus detachment of pieces of material. For a long time it was debated whether cavitation damage is caused by the shock waves when the remnant cloud reaches its minimum volume, or by microjets. It was shown, however, that it is possible that both microjets and shock waves can cause cavitation damage [11].

2 RAYLEIGH-PLESSET EQUATION

In order to describe practical cases of bubble dynamics, such as bubble formation, bubble collapse and bubble oscillations, it is necessary to make certain assumptions that will simplify the process of deriving the mathematical model. Main assumptions for the bubble and surrounding liquid include:

- Liquid is incompressible, i.e. its density ρ_L is constant.
- Dynamic viscosity of the liquid μ_L is assumed to be constant and uniform.
- Gravity is neglected.
- Temperature far from the bubble T_∞ is assumed to be constant.
- Pressure far from the bubble $p_\infty(t)$ is either assumed to be constant or it is controlled.
- Air content of the bubble is homogeneous.
- Temperature $T_B(t)$, and pressure $p_B(t)$ within the bubble are always uniform.

2.1 Generalised Rayleigh-Plesset equation

A spherical bubble of radius $R(t)$ is considered where t is time, in an infinite domain of liquid. As shown in the Figure 2.1, radial position within the liquid is denoted by the distance r, from the centre of the bubble. The pressure, radial outward velocity and temperature within the liquid are denoted as $p(r,t)$, $u(r,t)$ and $T(r,t)$, respectively.

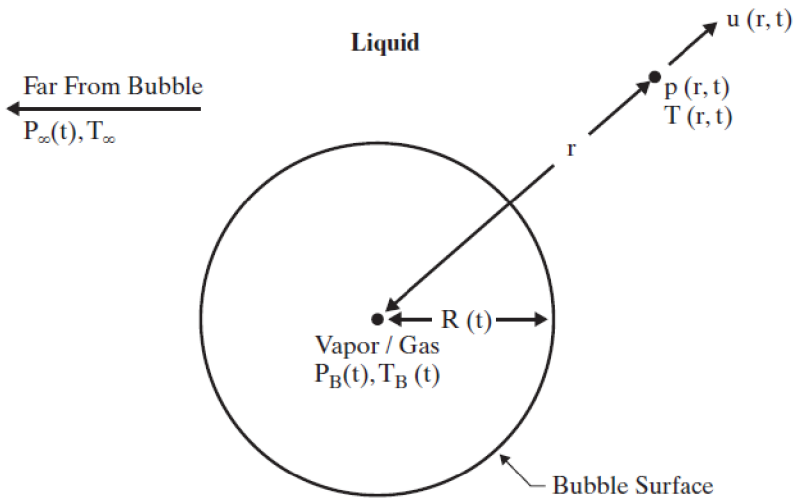

Figure 2.1 Schematic of a spherical bubble in an infinite liquid [2]

Conservation of mass requires that the radial outward velocity must be inversely proportional to the square of the distance from the centre of the bubble. Letting *F(t)* be a function of time, it is obtained:

$$u(r,t) = \frac{F(t)}{r^2} \tag{2.1}$$

If there is no mass transport across the bubble surface, radial outward velocity is equal to the change of radius with time, and therefore:

$$F(t) = R^2 \frac{dR}{dt} \tag{2.2}$$

Since liquid is assumed to be Newtonian, the Navier-Stokes equation for motion in the *r* direction is given as:

$$-\frac{1}{\rho_L}\frac{\partial p}{\partial r} = \frac{\partial u}{\partial t} + u\frac{\partial u}{\partial r} - \nu\left[\frac{1}{r^2}\frac{\partial}{\partial r}\left(r^2\frac{\partial u}{\partial r}\right) - \frac{2u}{r^2}\right] \tag{2.3}$$

Substituting *u* from equation 2.1 into equation 2.3 gives:

$$-\frac{1}{\rho_L}\frac{\partial p}{\partial r} = \frac{1}{r^2}\frac{dF}{dt} - \frac{2F^2}{r^5} \tag{2.4}$$

if viscous terms are disregarded. By applying condition $p \to p_\infty$ as $r \to \infty$, equation 2.4 can be integrated to obtain:

$$\frac{p - p_\infty}{\rho_L} = \frac{1}{r}\frac{dF}{dt} - \frac{1}{2}\frac{F^2}{r^4} \qquad 2.5$$

The reason viscous terms are disregarded in equation 2.4 is that the only viscous contribution to the Rayleigh-Plesset equation arises from the dynamic boundary condition at the interface. It is then necessary to obtain this dynamic boundary condition by considering an infinitely thin lamina containing a portion of the bubble surface, as shown in Figure 2.2.

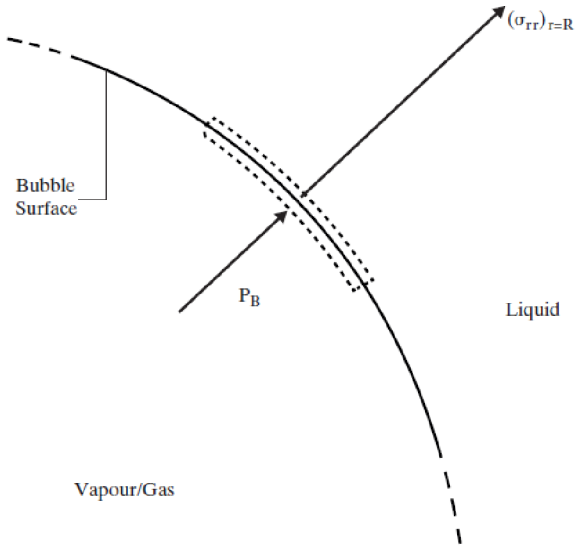

Figure 2.2 Lamina on the spherical bubble surface [2]

The net force acting on this lamina is:

$$(\sigma_{rr})_{r=R} + p_B - \frac{2S}{R} \qquad 2.6$$

Since:

$$\sigma_{rr} = -p + 2\mu_L \frac{\partial u}{\partial r} \qquad 2.7$$

the force per unit area is:

$$p_B - (p)_{r=R} - \frac{4\mu_L}{R}\frac{dR}{dt} - \frac{2S}{R} \qquad 2.8$$

This force must be zero in case of no mass transport across the boundary, and after substitution of the value for $(p)_{r=R}$ from equation 2.5 with $F = R^2 dR/dt$ we obtain the generalised Rayleigh-Plesset equation for bubble dynamics:

$$\frac{p_B(t) - p_\infty(t)}{\rho_L} = R\frac{d^2R}{dt^2} + \frac{3}{2}\left(\frac{dR}{dt}\right)^2 + \frac{2S}{\rho_L R} + \frac{4\mu_L}{\rho R}\frac{dR}{dt} \qquad 2.9$$

or written in more common form as:

$$\frac{p_B(t) - p_\infty(t)}{\rho_L} = R\ddot{R} + \frac{3}{2}\dot{R}^2 + \frac{2S}{\rho_L R} + \frac{4\mu_L}{\rho}\frac{\dot{R}}{R} \qquad 2.10$$

Furthermore, it can be assumed that the bubble contains, alongside vapour, some contaminant gas whose partial pressure is p_{g0}. If there is no mass transfer of gas to or from liquid, it applies that:

$$p_B(t) = p_v(T_B) + p_{g0}\left(\frac{T_B}{T_\infty}\right)\left(\frac{R_0}{R}\right)^3 \qquad 2.11$$

For an inviscid liquid, the last term on the right-hand side of the equation 2.10 becomes zero. Since Rayleigh-Plesset equation can be solved only numerically in most of the cases, initial bubble radius, R_0 and bubble velocity at time $t = 0$, $\dot{R}(t=0)$ serve as initial conditions, thus obtaining following relation:

$$p_B(t=0) = p_\infty(t=0) + \frac{2S}{R_0} \qquad 2.12$$

where $p_B(t=0)$ denotes the ambient pressure of the liquid exerted on the bubble in the initial state. After making assumptions that gases inside the bubble are non-condensable, not experiencing phase transition, and follow the polytropic behaviour, the relation for the pressure inside the bubble can be obtained for time $t = 0$ as:

$$p_v(T_\infty) + p_B(t=0) = p_\infty(t=0) + \frac{2S}{R_0} \qquad 2.13$$

2.1.1 Bubble equilibrium

Equilibrium of a bubble can be obtained by setting all time derivatives in the Rayleigh-Plesset equation to zero and assuming that pressure, p_∞ is constant:

$$p_\infty = p_{g0}\left[\frac{R_0}{R}\right]^3 + p_v - \frac{2S}{R} \tag{2.14}$$

After solving this equation with respect to radius R, we can obtain the radius of equilibrium of a bubble. Bubble equilibrium is not always stable due to the existence of a minimum for the equilibrium curve. Critical radius R_c, and critical pressure p_c are given by:

$$R_c = \sqrt{\frac{3p_{g0}R_0^3}{2S}}$$
$$p_c = p_v - \frac{4S}{3R_c} \tag{2.15}$$

Critical radius and critical pressure depend on surface tension S and on the mass of non-condensable gas in the bubble.

2.1.2 Bubble growth

It is possible to simplify Rayleigh equation even more if the effects of surface tension, viscosity and non-condensable gas are neglected, as it is the case when the bubble is much bigger than the original nucleus. If liquid pressure is smaller than vapour pressure, the bubble will grow and the asymptotic growth rate for large radii is given as:

$$\dot{R} \cong \sqrt{\frac{2}{3}\frac{p_v - p_\infty}{\rho}} \tag{2.16}$$

2.1.3 Collapse of a pure vapour bubble

In case when applied pressure is higher than the vapour pressure, the bubble radius decreases and that phase is known as the collapse phase. If assumptions of no

viscosity, non-condensable gas and surface tension are still valid, the interface velocity during the collapse is given as:

$$\dot{R} \cong -\sqrt{\frac{2}{3}\frac{p_\infty - p_v}{\rho}\left[\left(\frac{R_0}{R}\right)^3 - 1\right]} \qquad 2.17$$

By integrating this equation, we can obtain a so-called Rayleigh time, which is time needed for the bubble to completely disappear, i.e. until $R = 0$.

2.1.4 Bubble resonance frequency

Non-condensable gas contained in the bubble may be expressing elastic behaviour which could induce bubble oscillations. It is possible to predict the pulsating behaviour of a bubble and compute its resonance frequency from Rayleigh-Plesset equation:

$$f_0 = \frac{1}{2\pi R_0}\sqrt{\frac{1}{\rho}\left[3k\left(p_{\infty 0} - p_v + \frac{2S}{R_0}\right) - \frac{2S}{R_0}\right]} \qquad 2.18$$

2.2 Modifications of Rayleigh-Plesset equation

In case when a bubble collapse is studied, it may be necessary to adjust Rayleigh-Plesset equation and give importance to some additional phenomena, such as:

- Heat transfer between the gas within the bubble and the liquid. This is of particular importance in cases when bubble collapse causes light emission, a so-called phenomenon of sonoluminescence, described in detail by Jarman [12].
- Liquid compressibility that causes shock waves during the final stages of bubble collapse.
- Vapourisation that causes thermodynamic effect, i.e. temperature gradients between the bubble and the liquid.

Incompressibility of studied liquid is one of the main assumptions made in the beginning of derivation of Rayleigh-Plesset equation, but it may be the wrong approach in some cases. When including compressibility effect, equation of state is needed to account for density variation.

2.2.1 Models by Herring and Trilling

Herring [13] was the first author who introduced liquid compressibility into the bubble dynamics by assuming a constant value of velocity of sound in the liquid. Afterwards, Trilling [14] investigated the pressure and velocity field around collapsing bubble. Both of the mentioned estimates are suitable in the cases where the liquid velocity is much smaller than the velocity of sound in the liquid. Herring's model involves that the liquid velocity at the bubble surface be slower than the constant velocity of sound in the liquid, c_0:

$$R\left(1-\frac{2\dot{R}}{c_0}\right)\frac{d\dot{R}}{dt}+\frac{2}{3}\left(1-\frac{4\dot{R}}{3c_0}\right)\left(\frac{dR}{dt}\right)^2=\frac{R\dot{R}}{\rho c_0}\left(1-\frac{\dot{R}}{c_0}\right)\frac{dp_R}{dR}+\frac{p_R-p_\infty}{\rho_\infty} \qquad 2.19$$

The pressure at the bubble wall, p_R, can be obtained from momentum balance as:

$$p_R=p_B-\frac{2S}{R}+\frac{4\mu_L}{R}\frac{dR}{dt} \qquad 2.20$$

2.2.2 Gilmore's model

Gilmore [15] used the Kirkwood-Bethe hypothesis to describe the cavitation bubble for arbitrary velocity, taking into account compressibility of the liquid:

$$R\left(1-\frac{\dot{R}}{c}\right)\frac{d\dot{R}}{dt}+\frac{2}{3}\left(1-\frac{\dot{R}}{4c}\right)\left(\frac{dR}{dt}\right)^2=H\left(1-\frac{\dot{R}}{c}\right)\frac{dp_R}{dR}+\frac{R}{c}\left(1-\frac{\dot{R}}{c}\right)\dot{R}\frac{dH}{dR} \qquad 2.21$$

where the undissipated enthalpy, H, is defined by:

$$H=\int_{p_\infty}^{p_R}\frac{dp}{\rho} \qquad 2.22$$

Detailed comparison between results obtained by Rayleigh's, Herring's, and Gilmore's models of gas bubbles can be found in article by Vokurka [16]. Even

though Gilmore and the Herring and Trilling models are similar, the Gilmore model shows less violent bubble collapse.

2.3 Runge-Kutta methods

Numerical method used for solving Rayleigh-Plesset equation in this case is Runge-Kutta method of fourth order. It was previously shown by Tey, et al. [17] that models based on Runge-Kutta methods are capable of handling dramatic changes of bubble radius with satisfactory computation speed. Following subsection will describe the theory behind the method and its advantages.

Runge-Kutta (RK) methods attain the accuracy of a Taylor series approach without need for calculation of higher derivatives [18]. General form of RK method is:

$$y_{i+1} = y_i + \varphi h \tag{2.23}$$

where h is called the step-size, i.e. the length of the interval over which the approximation is made, and φ is called an increment function that can be written as:

$$\varphi = a_1 k_1 + a_2 k_2 + \cdots + a_n k_n \tag{2.24}$$

where a's are constants and k's are:

$$k_1 = f(t_i, y_i) \tag{2.25}$$

$$k_2 = f(t_i + p_1 h, y_i + q_{11} k_1 h) \tag{2.26}$$

$$k_3 = f(t_i + p_2 h, y_i + q_{21} k_1 h + q_{22} k_2 h) \tag{2.27}$$

$$k_n = f(t_i + p_{n-1} h, y_i + q_{n-1,1} k_1 h + q_{n-1,2} k_2 h + \cdots + q_{n-1,n-1} k_{n-1} h \tag{2.28}$$

where p's and q's are constants. It is obvious that the k's are recurrence relationships, i.e. k_1 appears in the equation for k_2, which then appears in the equation for k_3 and so on. This recurrence makes RK methods suitable for computer

calculations. First-order RK with *n=1* is essentially Euler's method. The most used RK methods are fourth order and the classical fourth-order RK method is given as:

$$y_{i+1} = y_i + \frac{1}{6}(k_0 + 2k_1 + 2k_2 + k_3)h \tag{2.29}$$

where:

$$k_0 = f(t_i, y_i) \tag{2.30}$$

$$k_1 = f(t_i + \frac{1}{2}h, y_i + \frac{1}{2}k_0 h) \tag{2.31}$$

$$k_2 = f(t_i + \frac{1}{2}h, y_i + \frac{1}{2}k_1 h) \tag{2.32}$$

$$k_3 = f(t_i + h, y_i + k_2 h) \tag{2.33}$$

Solvers based on Runge-Kutta methods have shown high computational accuracy and they were able to deal with the sharp rate of change of radius during bubble collapse and rebound stages. However, RK family solvers are computationally more expensive compared to Euler and 2nd order Taylor's method.

3 APPLICATION OF THE RAYLEIGH-PLESSET MODEL

After setting-up the necessary equations and selecting the proven numerical method for model development, it was possible to proceed to model development. Several software were considered, but computational power of MS Excel was deemed sufficient for further proceedings.

3.1 Verification of the Rayleigh-Plesset equation

Preliminary model's accuracy was determined using pre-existing experimental results and parameters stated in the Table 3.1:

Table 3.1 Fluid parameters and initial conditions

Name	Symbol	Value	Unit
Liquid density	ρ_L	9.98E+02	Pa
Vapourisation pressure	p_v	23.39E+02	Pa
Change of liquid pressure	dp_∞	4.00E+05	Pa
Liquid pressure	p_∞	1.00E+05	Pa
Frequency	ω	1.40E+04	Hz
Initial bubble radius	R_0	1.60E-05	m
Initial bubble velocity	dR_0/dt	0.00E+00	$m \cdot s^{-1}$
Ratio of specific heats	κ	1.00E+00	-
Surface tension	S	7.73E-02	$Pa \cdot m$
Dynamic viscosity	μ	1.00E-03	$Pa \cdot s$
Kinematic viscosity	ν	1.00E-06	$m^2 \cdot s^{-1}$

However, surface tension and fluid viscosity were to be included only in the second phase of model preparation. Bubble radius R_0 and bubble velocity dR_0/dt represent initial conditions necessary for solving this problem numerically. Driving mechanism of cavitation in this case was change of liquid pressure, given by dp_∞, where pressure variation is calculated as:

$$p_\infty(t) = p_\infty - dp_\infty \cdot sin\,(2\pi \cdot \omega \cdot t) \tag{3.1}$$

After calculating pressure, it was possible to calculate bubble radius over the same time period in which pressure is modified, using Runge-Kutta method.

Procedure starts by the standard Rayleigh-Plesset equation, disregarding surface tension *S* and liquid kinematic viscosity *ν*:

$$R\frac{d\dot{R}}{dt}+\frac{3}{2}\left(\frac{dR}{dt}\right)^{2}=\frac{p_b(t)-p_\infty}{\rho} \tag{3.2}$$

By dividing both sides of the equation by radius *R* we obtain:

$$\frac{d\dot{R}}{dt}+\frac{1}{R}\frac{3}{2}\left(\frac{dR}{dt}\right)^{2}+\frac{p_\infty-p_b(t)}{\rho} \tag{3.3}$$

Since equation 3.3 is a second order differential equation, in order for it to be solved it has to be transformed into a system of two first order ordinary differential equations (ODE):

$$\frac{dR}{dt}=z \tag{3.4}$$

$$\frac{dz}{dt}=-\frac{1}{R}\frac{3}{2}z^{2}-\frac{1}{R}\left(\frac{p_\infty-p_b(t)}{\rho}\right) \tag{3.5}$$

It is then possible to solve for coefficients k_0 through k_3, and l_0 through l_3, thus obtaining all the necessary coefficients for calculating bubble radius. Detailed calculation based on formulas given in subsection 2.3 is given in the APPENDIX A – Applying 4th order RK method to the system of equations.

After initial model was prepared, it was possible to develop a model that will take into account surface tension and liquid viscosity, and compare the results. Following results are obtained using model that includes effects of viscosity and surface tension. It is known that ideal liquid, compared to the viscous one, has higher collapse velocity. On the other hand, increase in surface tension causes collapse velocity to increase, however it decreases growth velocity.

Obtained pressure signal and bubble radius evolution are depicted in Figure 3.1 and Figure 3.2.

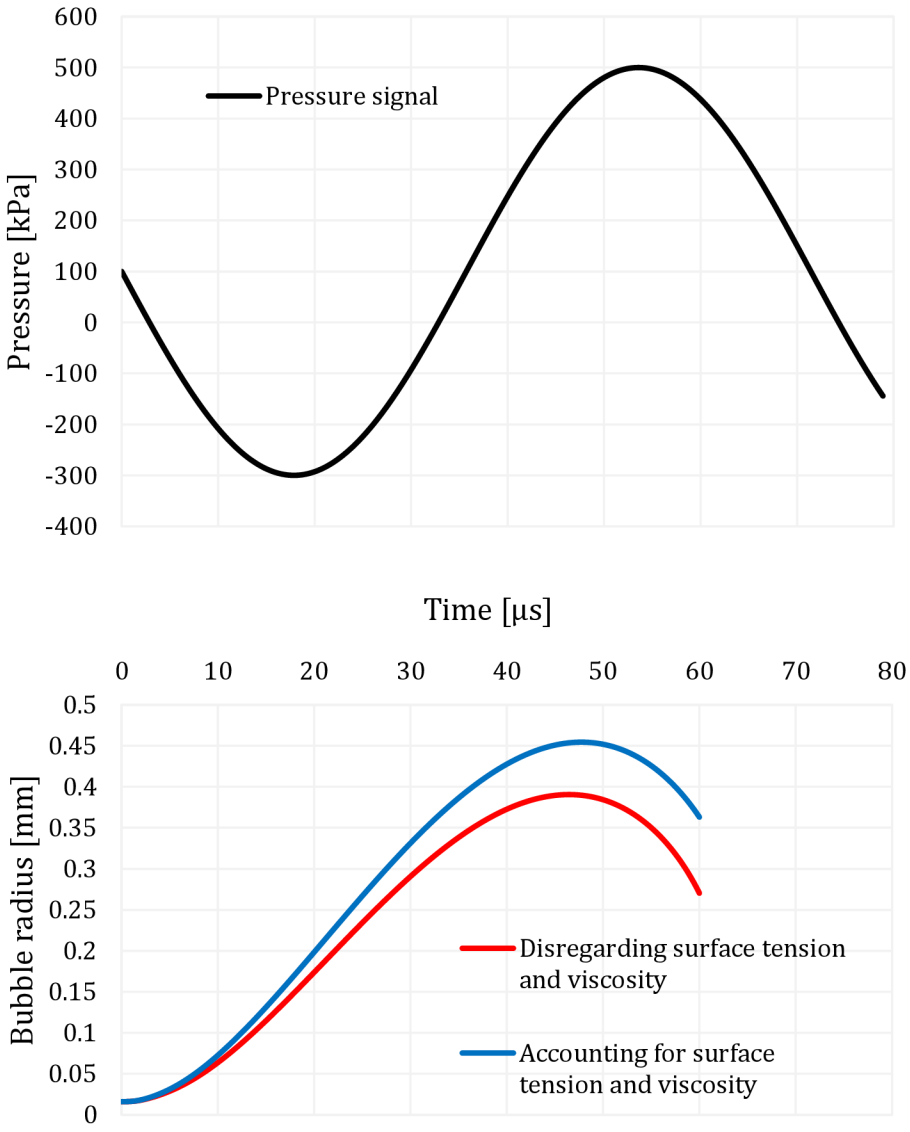

Figure 3.1 Calculated bubble radius as a function of change in pressure

The dependence of the bubble radius (bottom graph) and liquid pressure (top graph) on time are given in Figure 3.1. Initial decrease in pressure (up to 20 μs) causes rapid bubble expansion. Following the subsequent increase in pressure (after 20 μs), the bubble expansion velocity decreases to zero at the maximum bubble radius, R_m. At this point, bubble implosion starts. The unfinished numerical calculation is caused by the violent collapse velocity close to the final stage of collapse, which is the limitation of the incompressible model.

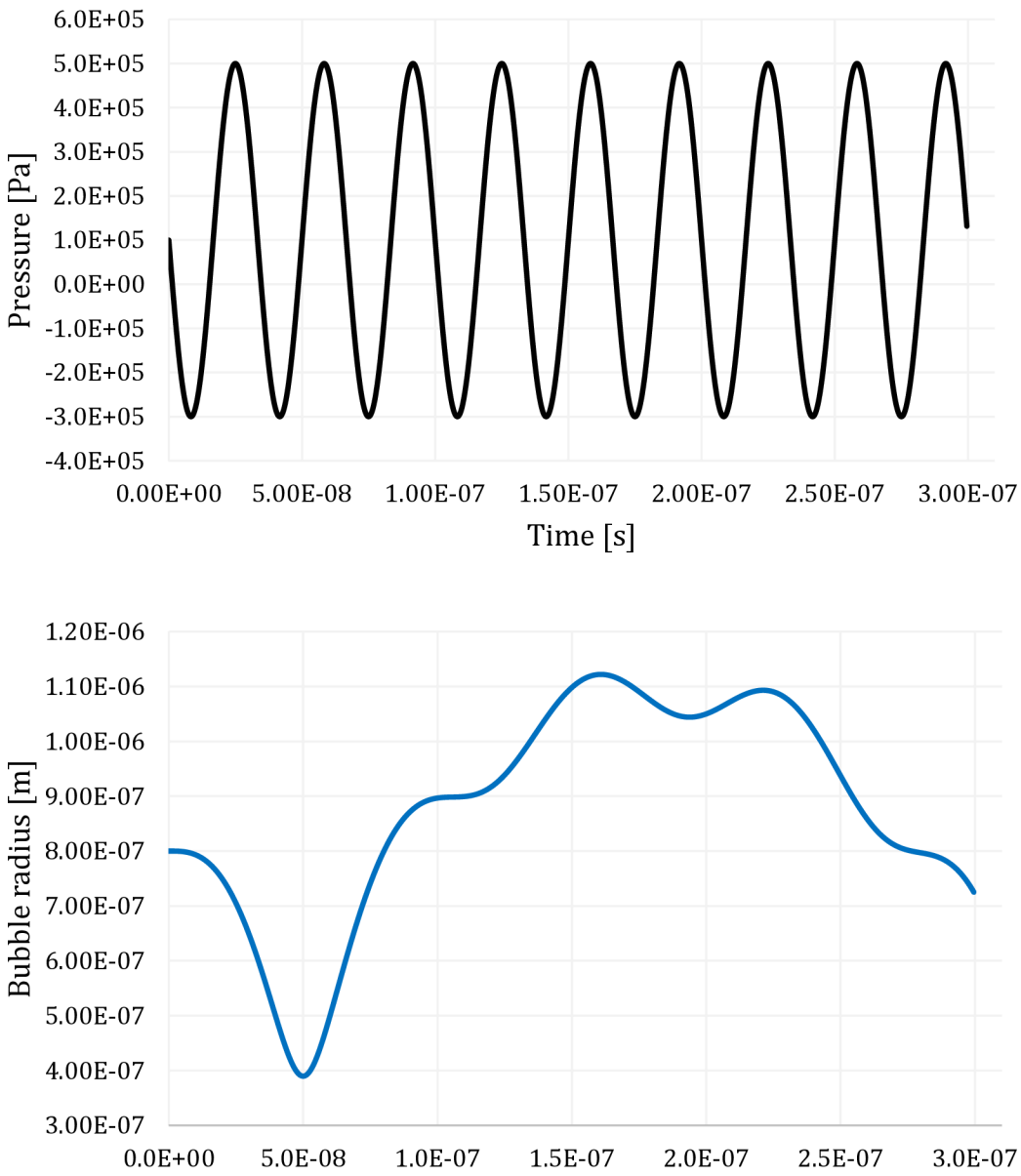

Figure 3.2 Influence of pressure of higher frequency ($9 \cdot 10^7$ Hz) on bubble radius

As presented in the Figure 3.2, if the frequency of the acoustic wave is greater than the resonant frequency of the bubble, it causes bubble not to fully collapse, but rather to behave in a way not typical for cavitation, i.e. to perform very complex oscillations.

Obtained signals were then compared to the signals from Brdička et al. [19], thus confirming they are the same, which indicates that the model of Rayleigh-Plesset equation works properly.

3.2 Testing the influence of the liquid properties on cavitation bubble dynamics using numerical model

In the following subsection, the model will be tested according to changes in different properties of the fluid and initial conditions, namely:

- initial bubble radius - Figure 3.3;
- pressure amplitude - Figure 3.4;
- viscosity - Figure 3.5;

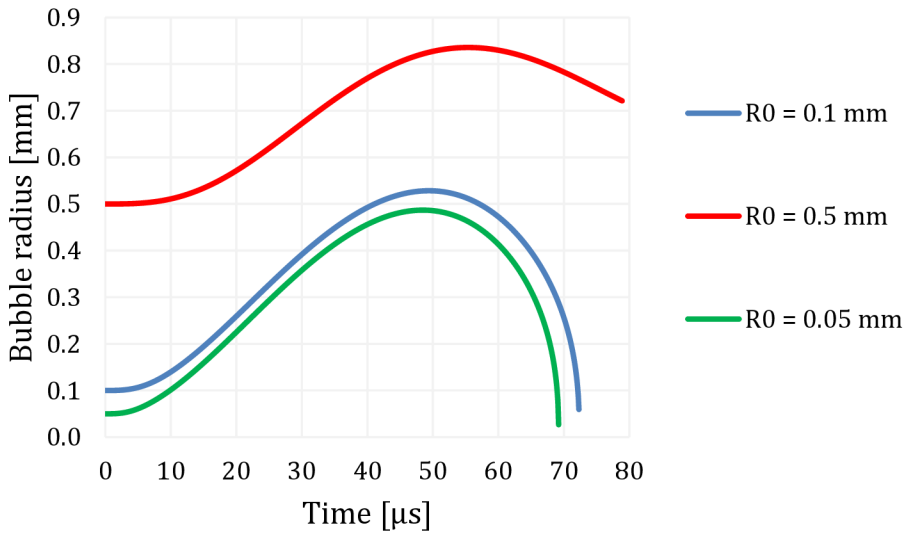

Figure 3.3 Influence of initial bubble radius on overall bubble growth

Figure 3.3 shows behaviour of the bubble radius dependent on initial bubble radius R_0. Increase in initial bubble radius causes higher values of maximum bubble radius, as well as longer time of bubble lifetime, which is in the case of $R_0 = 0.5$ *mm* again limited by the incompressible model. Contrary to this, bubbles with smaller initial radii are represented well by the model in the first phase of the bubble lifetime.

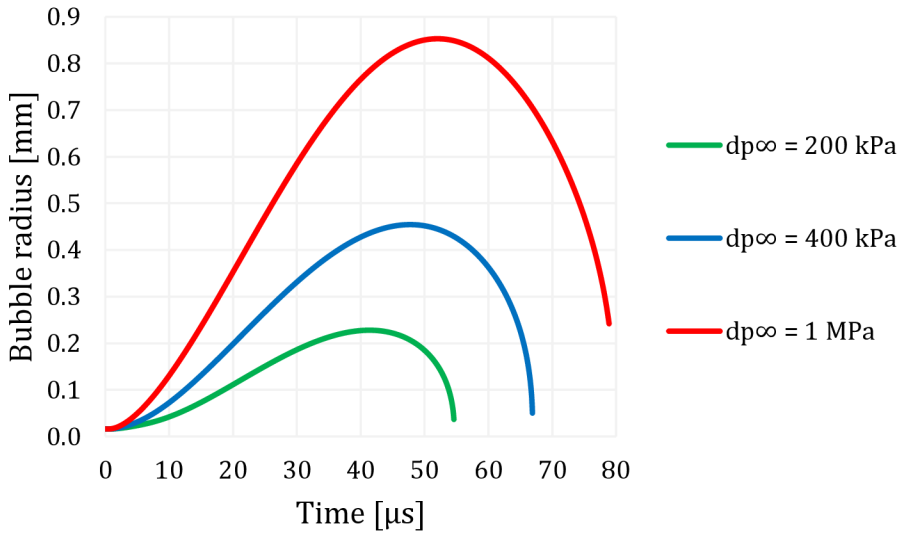

Figure 3.4 Influence of pressure amplitude on overall bubble growth

Figure 3.4 implies that another parameter that can increase maximum bubble radius and bubble lifetime is pressure amplitude. With an increase in bubble amplitude, maximum bubble radius increases significantly. The limitation is, however, again set by the incompressibility of the used model.

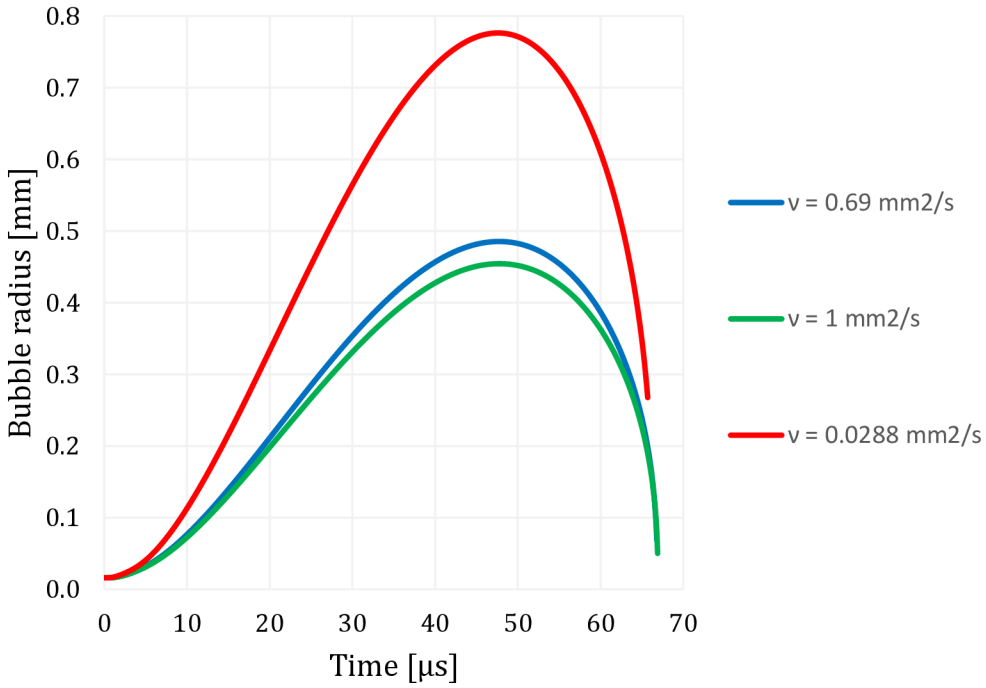

Figure 3.5 Influence of viscosity on overall bubble growth

As already mentioned, liquids with low viscosity achieve high collapse velocity. In Figure 3.5, it is seen that such liquids reach higher maximum bubble radius, as well, compared to, for example, liquid with the value of kinematic viscosity $\nu = 1\ mm^2/s$ (green curve).

In order to observe bubble behaviour under different conditions, the model will be tested and following parameters can be observed:

- maximum radius R_m
- velocity near collapse u_{col}
- pressure near collapse p_{col}

Results for velocity and pressure are normalised using equation 3.6, whereas values of radii are presented as absolute.

Dependence of bubble parameters on viscosity

Main influence of viscosity in a cavitation bubble is that viscous liquids have lower collapse velocity than ideal liquids. That is in contrast to surface tension, which increases collapse velocity, but lowers growth velocity.

Dependence of bubble parameters on initial bubble radius

Bubbles of following initial radii are observed: $R_{01} = 1.6 \cdot 10^{-5}\ m$, $R_{02} = 1 \cdot 10^{-4}\ m$ and $R_{03} = 1.6 \cdot 10^{-4}\ m$. Effect of initial bubble radius on overall growth and maximum radius is already shown in Figure 3.3. Figure 3.6, on the other hand, compares bubble normalised speed as a function of different initial bubble radii. Normalised bubble speed is calculated as follows:

$$u_{\text{normalised}} = \frac{u - u_{min}}{u_{max} - u_{min}} \qquad 3.6$$

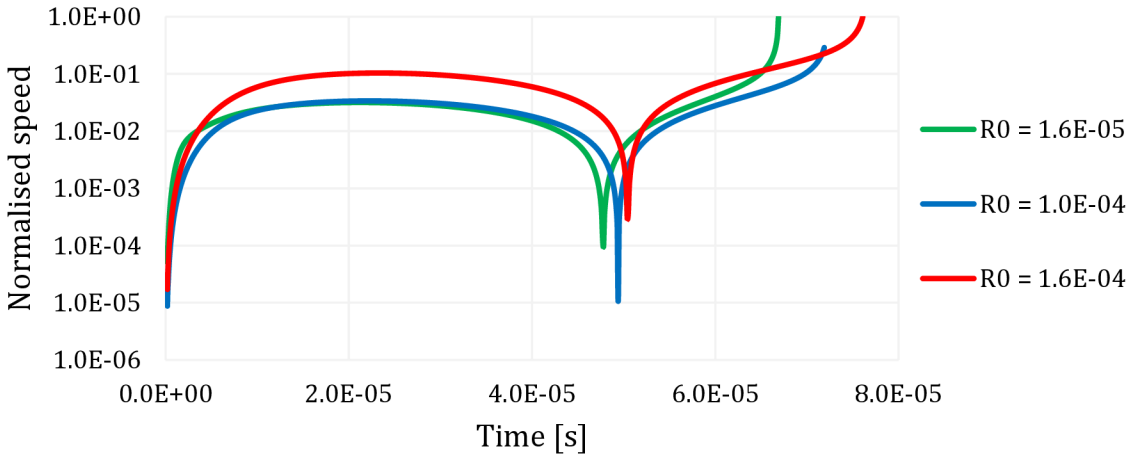

Figure 3.6 Dependence of bubble speed on initial bubble radius

From Figure 3.6 it is obvious that for higher values of initial bubble radius, final stage of bubble collapse is affected, i.e. normalised speed of value $u_{normalised} = 1$ occurs later. On the other hand, a decrease in initial bubble radius causes that maximum achievable speed obtained by the model occurs earlier.

Dependence of bubble parameters on pressure amplitude

Pressure amplitudes of following values are applied: $dp_\infty = 50\ kPa$, $dp_\infty = 200\ kPa$ and $dp_\infty = 400\ kPa$. As Figure 3.4 already shows dependence of bubble radius on pressure amplitude, following figures will show dependence of bubble velocity and pressure on the amplitude.

Similar to initial bubble radius, an increase in pressure amplitude applied to the liquid causes maximum (collapse) velocity to occur later, as seen in Figure 3.7. Furthermore, with increase in pressure amplitude, minimum value of bubble speed ($u = 0$ at R_m) occurs later.

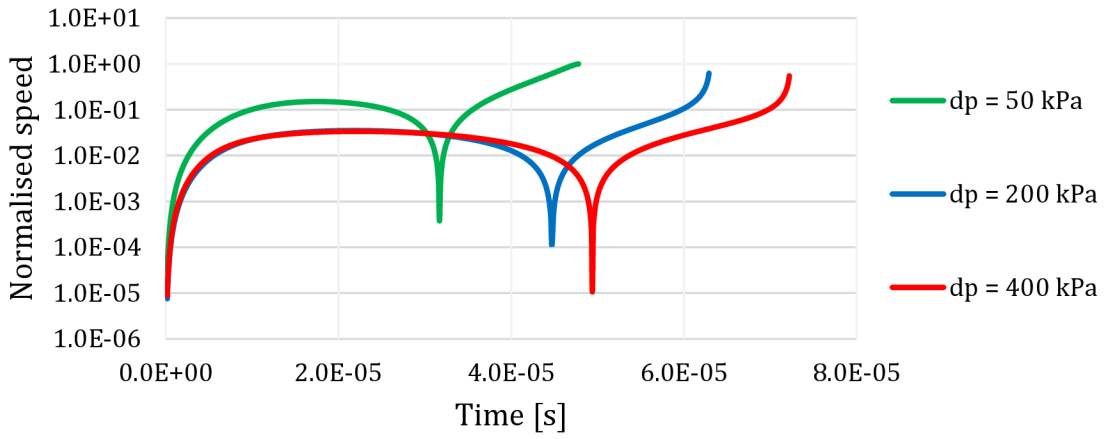

Figure 3.7 Dependence of bubble speed on pressure amplitude

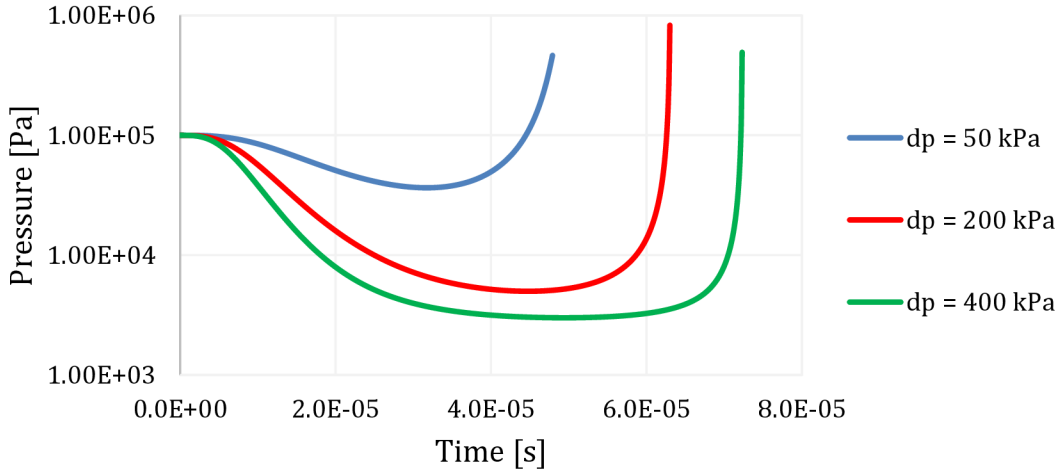

Figure 3.8 Dependence of bubble pressure on pressure amplitude

Figure 3.8 shows that with increase in pressure amplitude, maximum pressure in the bubble, i.e. pressure during the collapse stage, occurs later. Similarly, it is shown that by applying higher pressure amplitudes, minimum pressure in the bubble is affected as well.

3.3 Validation of the numerical model towards the available experiments

3.3.1 Available experiments

Prepared model of bubble dynamics was applied to two experiments – laser-induced bubble and spark-generated bubble. By collecting data on bubble diameter change in time, it was possible to compare experimental results to the results

obtained by the Rayleigh-Plesset model and thus see its level of accuracy, as well as potential shortcomings.

Laser-induced bubble

Cavitation induced by laser can be used to obtain controlled cavitation bubbles, utilised especially in medicine [20]. In order for laser induced cavitation bubble to be usable in such applications, it is necessary to examine conditions and parameters which will lead to repeatability of cavitation bubbles [21]**.** Different types of fluids could be used to explore dependency of bubble behaviour on fluid properties [6].

Experimental setup and results

Following part will describe the experiment performed to examine the impact of laser induced cavitation on the solid wall [22] to obtain the experimental data necessary for model application. Figure 3.9 shows the setup for the bubble measurement. Neodymium-doped Yttrium Aluminium Garnet (Nd:YAG) laser at the wavelength of 532 nm is focused into the water bath to generate cavitation bubbles. Laser beam of diameter 5 mm is expanded through a Galilean beam expander and focused through a gold mirror, and laser-induced breakdown (LIB) is generated out of optical axis. Optical measurement was based on the high speed photography using ultra-fast charge-coupled device (CCD) camera, and bubble collapse illumination was provided by the high power flash lamp in continuous mode. The acoustic measurement was performed using polyvinylidene fluoride (PVDF) film fixed on a movable frame submerged into the bath. The PVDF film was used to measure the local time exposure caused by the direct interaction of the film. Once the experimental data for values of bubble radius were obtained, it was possible to proceed to applying the existing model using these values. Since the model is intended for bubble collapses sufficiently far from the wall, bubble is generated at a distance almost five times higher than the value of its maximum radius ($\gamma = s/R_m = 4.6$).

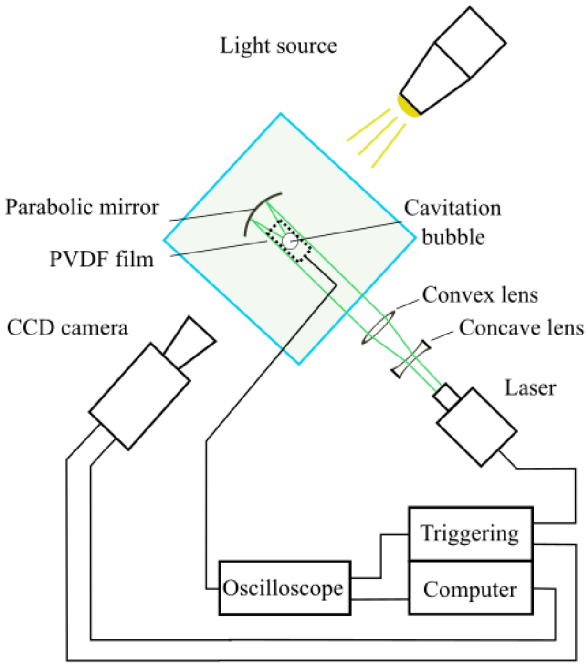

Figure 3.9 Experimental setup of laser-generated bubble
(note: PVDF film data is used only for the original experiment, not for this study – used with the permission of supervisor/author)

Figure 3.10 shows bubble growth and collapse as captured by the CCD camera, and Figure 3.11 shows values of radii obtained by the experiment.

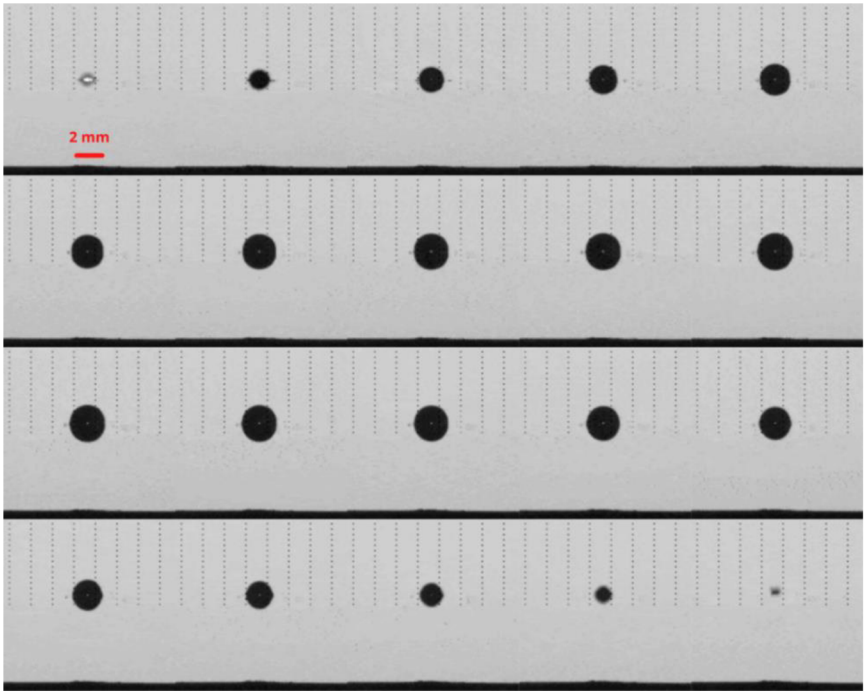

Figure 3.10 Visualisation of first two laser-induced cavitation bubble collapses (time between each frame is 5.55 μs)

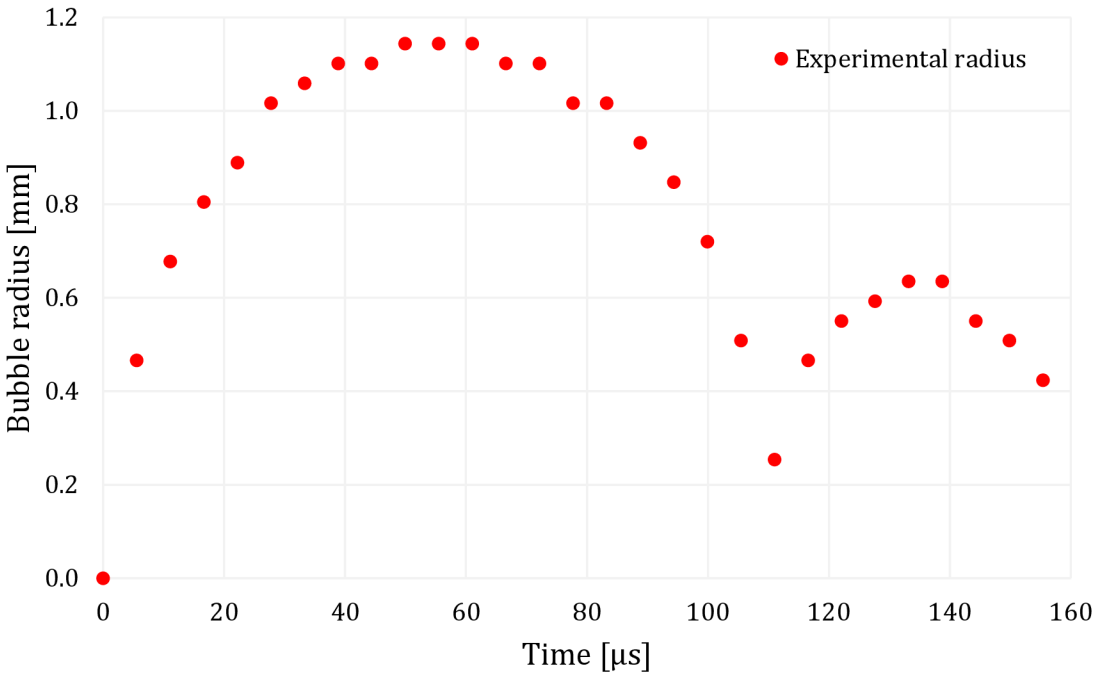

Figure 3.11 Radii obtained by the experiment – laser-generated bubble

High sphericity, seen in Figure 3.10, of this produced bubble means that the radius measurement would be more accurate than following spark generated bubbles (Figure 3.13 and Figure 3.15), meaning the model could be applied with smaller margin of error. This is due to the sufficient distance from the wall at which the bubble is generated. Figure 3.11 shows values of bubble radii in time obtained experimentally, with $R_0 = 0.47\ mm$ and $R_m = 1.14\ mm$. Second bubble growth is visible as well, showing second maximum bubble radius as approximately half the size of R_m.

Spark-generated bubbles

Second used experiment was based on generating cavitation bubbles by submerged electrodes. The results were then applied to the Rayleigh-Plesset model in order to establish its accuracy in this case. Spark-generated cavitation bubbles are useful for examination of a behaviour of a single bubble. In the work by Goh et al. [23], it was attempted to create consistently-sized spherical bubbles by applying low voltage. Similarly, the goal of this experiment was to apply low voltage for the purpose of creating spherical bubbles that would be measured easily and, more importantly, predicted well by the model. Since point of contact of electrodes is not close to a wall, it is expected that there will be no occurrence of re-entrant microjets.

Experimental setup and results

Experimental setup shown in the Figure 3.12 consists of following elements:

- CCD camera,
- high power flash lamp with magnifier,
- two touching needle-needle copper electrodes submerged in a tank,
- capacitor connected to the electrodes,
- signal generator,
- DC power supply,
- oscilloscope,
- PC equipped with image processing software,
- hydrophone for pressure signal measurement.

LED light is used to concentrate light on the electrodes inside the water bath while capturing it with camera. Firstly, electrodes are charged from the power supply, whilst capacitor relay is connected to the signal generator. Signal applied to relay switches the circuit, and after triggering the relay manually, the bubble is created at the contact point of electrodes. Images captured by the high-speed camera can be processed and the bubble diameter evolution can be measured. The experiment was performed under atmospheric pressure and at a room temperature.

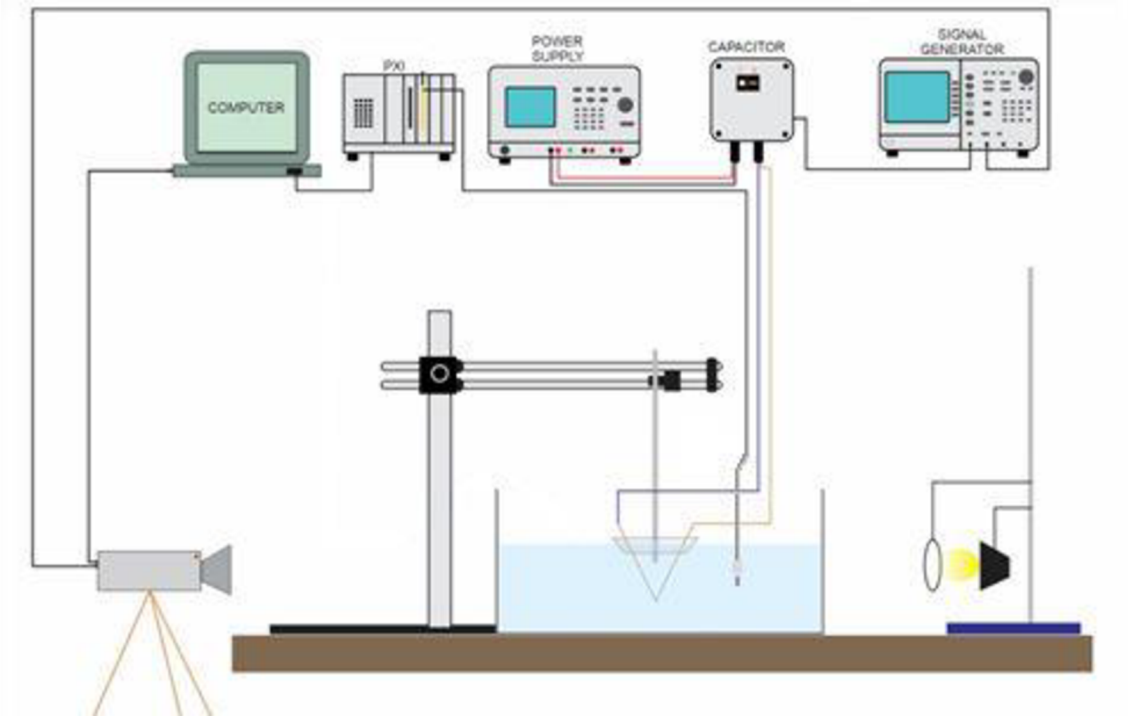

Figure 3.12 Experimental setup for spark-generated bubble

Unlike experiment with laser-induced bubble, this time bubble was generated far away from any flexible or rigid wall. This proved to generate spherical bubbles for the majority of the first growth and collapse. First bubble, seen in Figure 3.13 was generated without measuring pressure signal, whereas the second bubble, seen in the Figure 3.15, had a hydrophone included in the setup in order to obtain pressure oscillations. The experiments were carried out with tap water. The first bubble shows fairly spherical growth and relatively violent collapse. Ideally, wires should be touching only at their ends, otherwise another, smaller bubble will be generated at the end of the overhanging wire, which can be seen in the third image of the first row in Figure 3.13. Immediately after capturing the bubble, the scale for subsequent measuring of the bubble radius was captured by taking an image of a ruler with the same camera distance. This way, it was possible to convert between the number of image pixels (100 x 100) and distance in millimetres. In total, 140 images were taken in each measurement, one each 0.1 milliseconds.

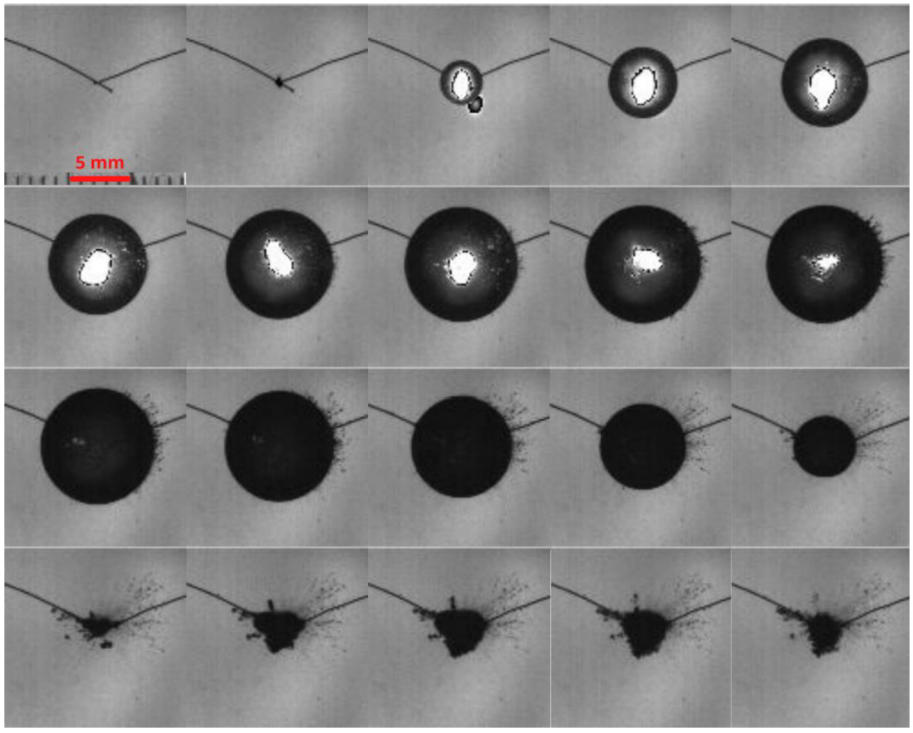

Figure 3.13 Visualisation of first two cavitation bubble collapses – first spark-generated bubble (time between each frame is 100 μs)

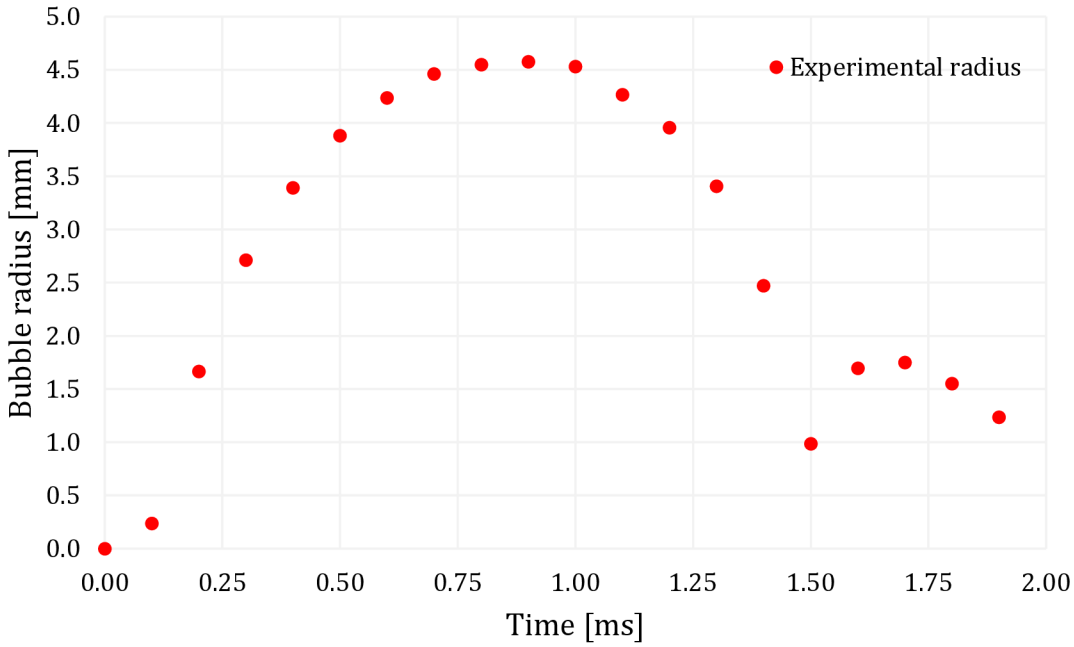

Figure 3.14 Radii obtained by the experiment - first spark-generated bubble

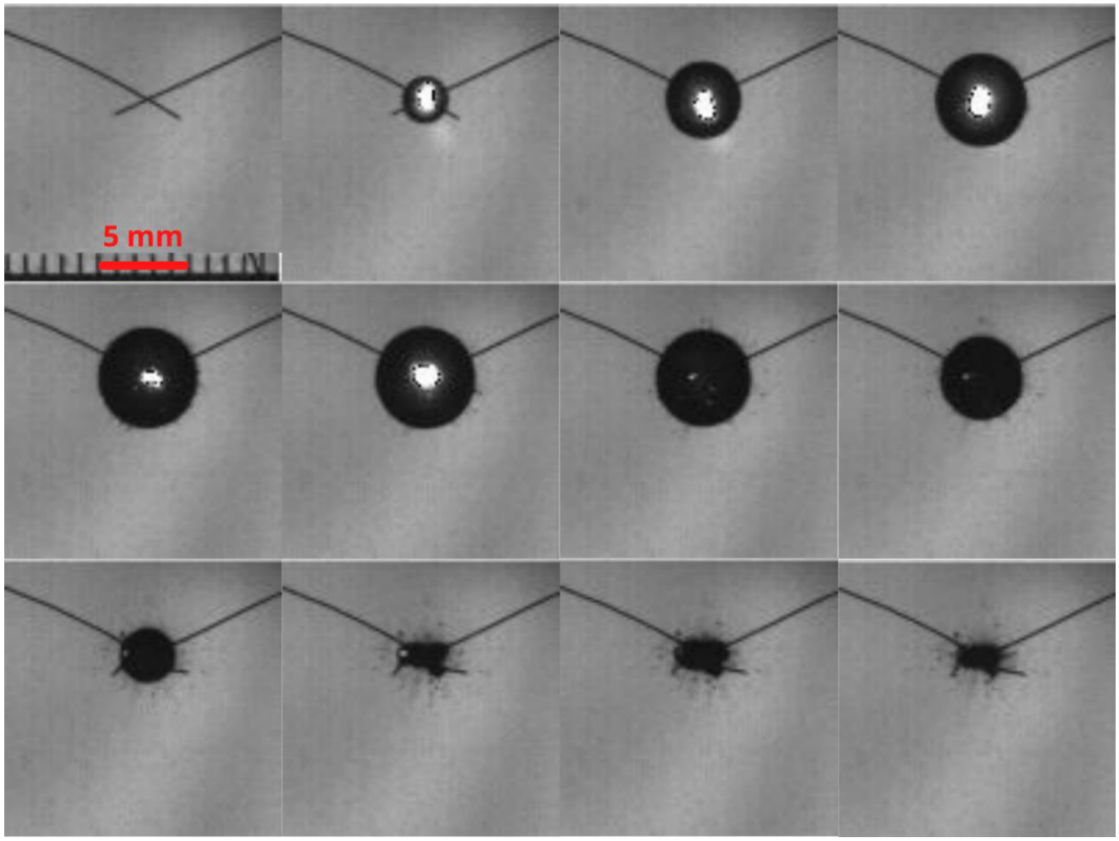

Figure 3.15 Visualisation of first two cavitation bubble collapses – second spark-generated bubble (time between each frame is 100 μs)

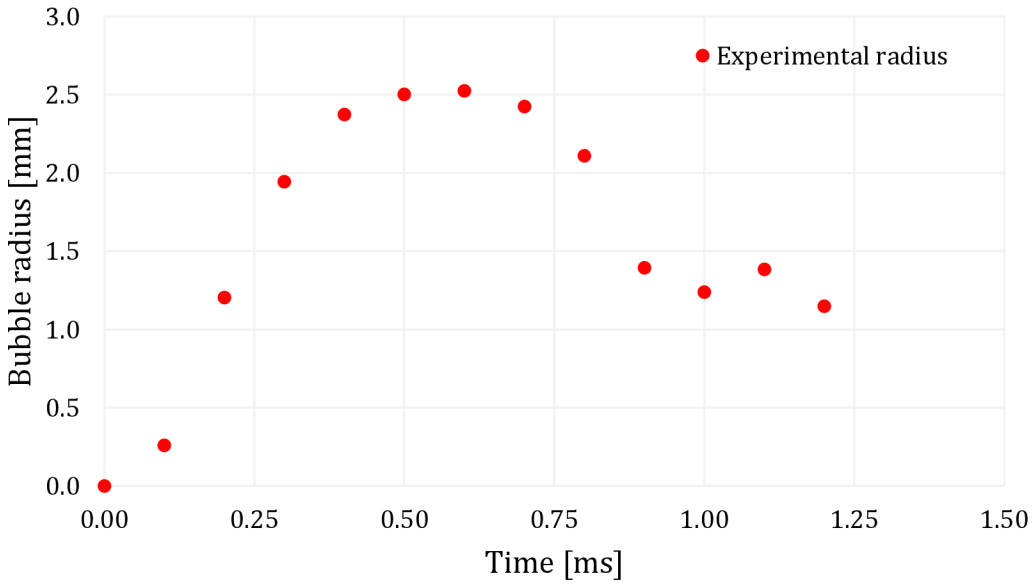

Figure 3.16 Radii obtained by the experiment - second spark-generated bubble

It can be seen that the bubble in Figure 3.15 has smaller maximum radius, which is presumably due to the quality of soldering connection between the wire and the electrode. Unlike laser-induced bubble, spark-generated bubbles tend to disintegrate after the first collapse (last rows in both Figure 3.13 and Figure 3.15), causing higher errors of radius measurement and model applicability. Values obtained experimentally are presented in Figure 3.14 and Figure 3.16, and show measured values of radii. However, bubble shapes after first collapse are not spherical which is due to disintegration of the bubbles during the rebound stage.

Bubble collapse time

Experimental results presented in subsection 3.3.1 can be used to test against another relation, namely collapse time, which is the time it takes for the bubble to collapse from maximum radius R_m to the minimum radius.

As previously mentioned, equation 2.17 can be integrated, thus obtaining the so-called Rayleigh time, or the time of the bubble collapse, given as:

$$\tau_{Ra} = 0.915 \cdot R_0 \cdot \sqrt{\frac{\rho}{p_\infty - p_v}} \qquad 3.7$$

where the constant 0.915 comes from the Gamma function. Using this equation, obtained experimental values can be compared to the theoretical ones. Comparison for all three bubble collapses presented in this research is given in the Table 3.2.

Table 3.2 Comparison of experimental collapse time and Rayleigh time

Bubble	**Time of the collapse (experimental) [μs]**	**Rayleigh time [μs]**	**Error [%]**
Laser-induced	56	50	9
Spark-generated (first)	600	477	21
Spark-generated (second)	400	366	8

3.3.2 Application of the Rayleigh-Plesset model to the experiments

Laser-induced bubble

In order not to model plasma distribution directly, it is necessary to simulate it by the growing bubble radius, as done by Vogel [25]. Simulation begins at an initial bubble radius $R_0 = R_{0a}$ which is identical to the experimentally determined maximum plasma size. Maximum bubble radius at the end of the pulse R_{0b} will be experimentally obtained as well. From this, it is possible to develop the expression for the evolution of bubble radius during the laser pulse:

$$R_0(t) = \left(R_{0a}^3 + \frac{R_{0b}^3(t) - R_{0a}^3}{2\tau_{La}} \left[t + \frac{\tau_{La}}{\pi} sin\left(\frac{\pi}{\tau_{La}} t \right) \right] \right)^{\frac{1}{3}} \qquad 3.8$$

where τ is the duration of time pulse for the bubble to grow from R_{0a} to some radius R_{0b}. Boundary and initial conditions necessary to solve this problem numerically are obtained by the experiment described in subsection 3.3.1. Maximum plasma size represents first initial condition, i.e. the initial bubble radius R_{0a}. In order to reach first maximum bubble radius, R_m that has already been determined experimentally, the value of R_{0b} needed to be adjusted several times.

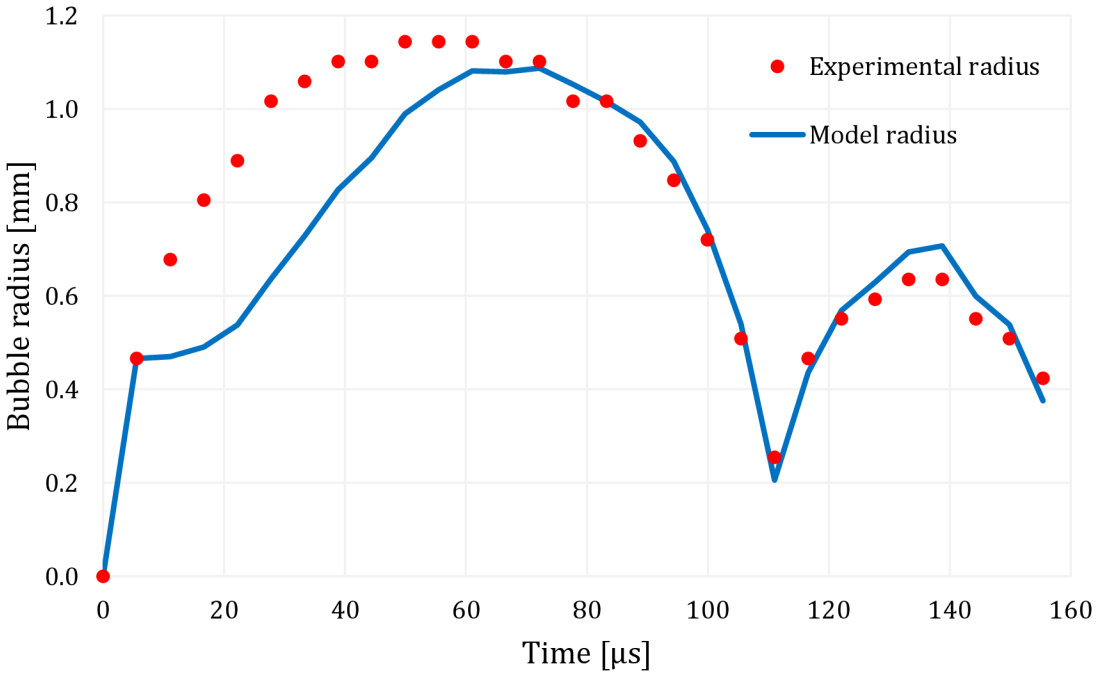

Figure 3.17 Comparison of radii obtained by the experiment and by the model – laser-generated bubble

Presented in Figure 3.17, comparison of radii obtained experimentally and by the model shows the disagreement of the results most significantly during the initial growth phase (from 0 to 70 μs). While values of radii are comparable, their occurrence in time does not coincide during the mentioned phase. However, during the rebound phase (from 110 to 160 μs), data obtained are in good agreement. The most evident shortcoming of the results obtained by the model, i.e. initial growth phase could be due to the initial bubble radius used.

Spark-generated bubble

After gathering all the necessary images (Figure 3.13 and Figure 3.15), first two bubble growths were extracted and bubble radii were measured at each of the selected time steps using the aforementioned scale. It could then be proceeded to the comparison of experimental results to the Rayleigh-Plesset model – firstly inputting the initial bubble radius R_0 and maximum radius R_m.

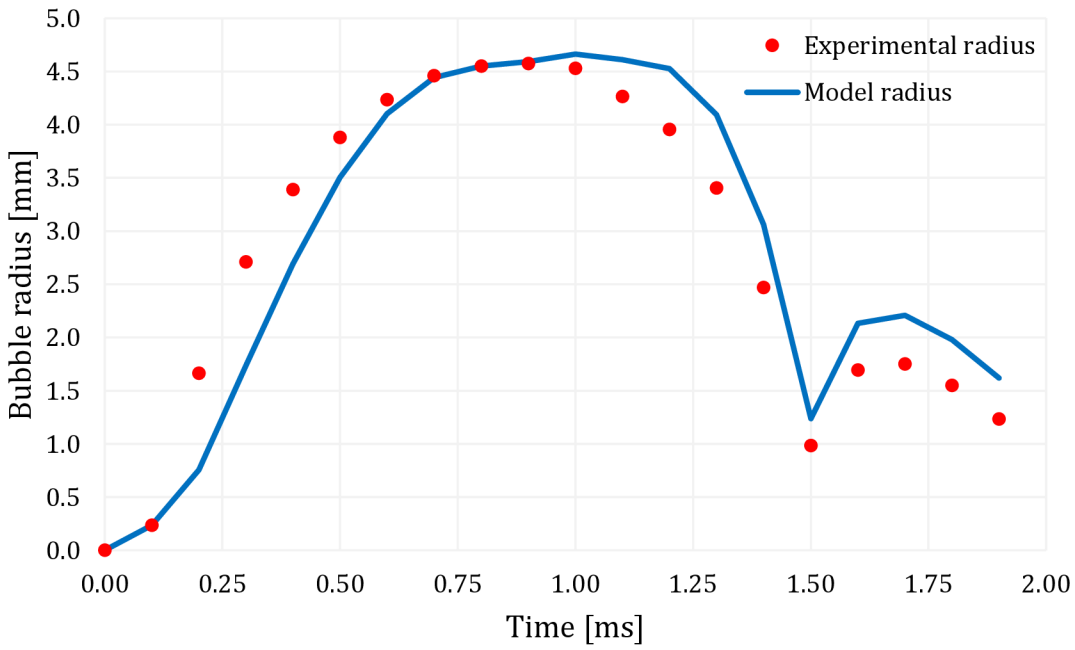

Figure 3.18 Comparison of radii obtained experimentally and by the model – first spark-generated bubble

Due to bubble symmetry observable from the gathered images, radii in either direction could be chosen for the radius measurement and model application. In this case, values of radii in horizontal direction were taken. From Figure 3.18 it can be observed that the radii obtained by the model are somewhat more accurate in this

case, compared to results obtained in the case of laser-generated bubble (Figure 3.17). This time, however, the data are not in as good agreement during the rebound phase as in the case of laser-induced bubble. Furthermore, during the initial growth phase (from 0.25 to 0.6 ms), values of radii tend to be shifted in time for some 0.1 ms.

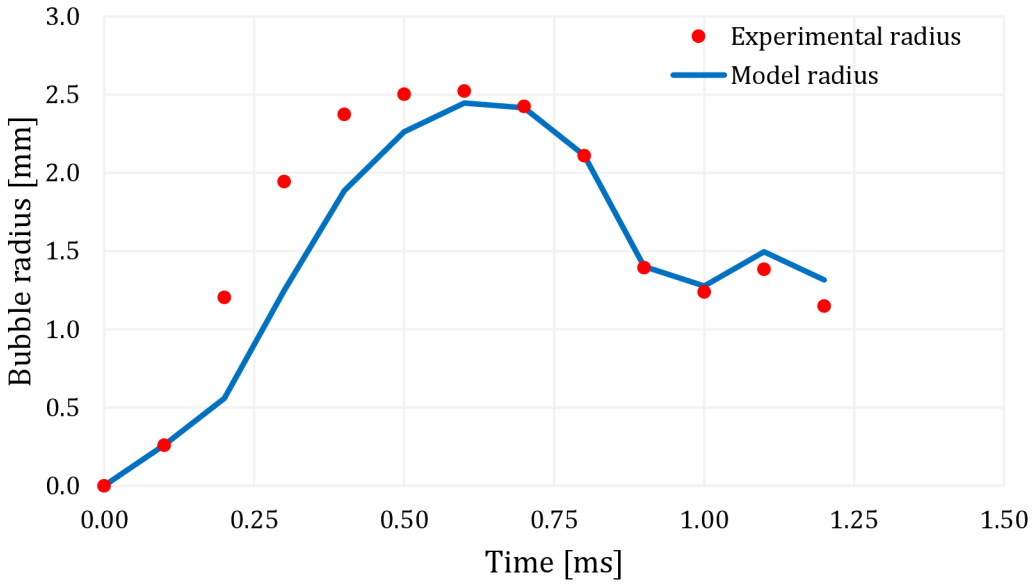

Figure 3.19 Comparison of radii obtained experimentally and by the model - second spark-generated bubble

As the maximum radius of bubble shown in Figure 3.19 is almost half the size of the bubble from Figure 3.18, its rebound is captured only during 3 frames, thus causing the experimental results during this phase insufficient for correct model application.

Oscillating period of a bubble is based on its maximum radius R_m, and collapse that finalises with the minimum radius. R_m is reached after 0.6 ms, and the collapse occurs during the next 0.4 ms, after which bubble is disintegrated and any radius measurement would come with significant error margin.

It can be concluded that the data obtained by the model are in better agreement with spark-generated bubble experiments because the initiation of bubble growth in this case is slower than in the case of laser-induced bubble growth.

As mentioned in subsection 3.3.1, second bubble experiment was conducted with the addition of hydrophone, a device based on a piezoelectric transducer that generates an electric potential when subjected to a pressure change. Signal obtained by the used hydrophone can be seen in Figure 3.20, and it clearly shows pressure amplitudes exactly at the time of bubble formation (initial spike just before 1 ms), as well as the first (pressure amplitude) and second bubble collapse that followed immediately.

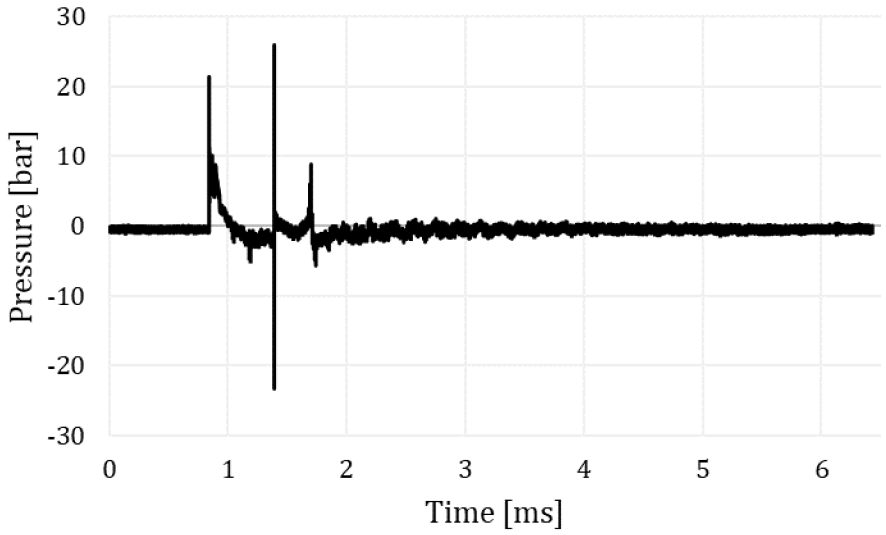

Figure 3.20 Pressure signal obtained by a hydrophone

4 POSSIBILITY OF USING THE MODEL FOR CAVITATION EROSION PREDICTION

Since cavitation erosion is closely connected to the pressure in the final stages of the bubble collapse, obtained data can be used to calculate pressure inside the bubble which will represent the potential of the cavitation erosion using:

$$p_{B,final} = p_v + p_{g0}\left(\frac{R_0}{R_{final}}\right)^{3k} \tag{4.1}$$

Furthermore, bubble and shockwave energy can represent the potential of cavitation erosion. An energy approach as a method for prediction of cavitation erosion is explained in detail in work by Avellan & Dupont [24]. Energy for the bubble growth from the initial radius to the maximum radius is expressed as:

$$E_m = \int_{R_0}^{R_m} 4\pi R^2 (p_\infty - p_v) dR = \frac{4\pi(p_\infty - p_v)}{3}[R_m^3 - R_0^3] \cong \frac{4\pi(p_\infty - p_v)}{3} R_m^3 \tag{4.2}$$

Equation 4.2 can also be used to derive the relation for the secondary shockwave generated between the first bubble contraction and secondary expansion:

$$E_{1shock} = E_{1m} - E_{2m} = \frac{4\pi(p_\infty - p_v)}{3}(R_{1m}^3 - R_{2m}^3) \tag{4.3}$$

Table 4.1 shows values of bubble and shockwave energy, as calculated from the experimentally obtained results and by the model.

Table 4.1 Comparison of results on collapse pressure, and bubble and shockwave energy obtained from experimental and model results

Value/experiment	**Laser-generated**	**Spark-generated (first)**	**Spark-generated (second)**
Experimental pressure in the bubble at the collapse [kPa]	604.13	474.03	91.96
Model pressure in the bubble at the collapse [kPa]	755.70	437.72	63.64
Experimental bubble energy E_m [mJ]	0.61	39.17	6.59
Model bubble energy E_m [mJ]	0.53	41.48	5.99
Experimental shockwave energy E_{1shock} [mJ]	0.51	36.98	5.49
Model shockwave energy E_{1shock} [mJ]	0.38	37.01	4.62

5 CONCLUSION

This study researched on the capabilities of Rayleigh-Plesset equation and the applicability of Runge-Kutta method to it. Rayleigh-Plesset equation was described in detail, as well as the theoretical background of it. Furthermore, several modifications of the equation are mentioned, namely models that take into account liquid compressibility or heat transfer.

After setting up necessary equations as a background, and describing some of the accompanying phenomena, it was possible to proceed to developing the model. Among many numerical methods available, Runge-Kutta method of fourth order was selected due to its robustness and history of application in similar researches. Detailed explanation of the process of solving a system of two first order differential equations is given, accompanied by an example of solving a first time step of Rayleigh-Plesset equations for a case without accounting for viscosity and surface tension (appendix).

In order to verify results obtained by the model, it was necessary to compare the results of a cavitation bubble radius development induced by a pressure pulse. Existing numerical results were taken for comparison, thus confirming the validity of the model in a case when surface tension and viscosity terms are disregarded.

Furthermore, it was possible to modify certain fluid parameters and initial conditions, such as viscosity, pressure, surface tension, along with initial bubble radius; with the aim of exploring influence of those variables on the bubble dynamics.

After verifying the results of a model, further model application was possible. It was decided that the model could be applied to two experiments – laser-induced cavitation bubble, and spark-generated cavitation bubble. As for the laser-induced bubble experiment, results were provided by the thesis supervisor from the previous experiment, whereas spark-generated bubble experiment could be performed during the time of the research. Experimental results were analysed and several important parameters were extracted, namely bubble diameters and the time, along with the images necessary for presentation purposes.

As all the necessary data for model validation was obtained, it was possible to proceed to the comparison of results obtained experimentally and by the model. Model proved to be robust, albeit with a few flaws regarding representing the initial phase of first bubble growth, especially in the case of laser-induced bubble. As for the spark-generated bubble, major obstacle was proved to be the number of time-steps, which affected the quality of model results.

Furthermore, applicability of the model for the erosion prediction was examined. In terms of model usability, it was concluded that bubble energy, shock wave energy and bubble pressure at the collapse represent parameters that could be used for erosion prediction.

Finally, it can be concluded that Rayleigh-Plesset equation, together with proper numerical method, despite its relative simplicity, is still able to provide researchers with excellent results, saving the time and means necessary for obtaining experimental results.

REFERENCES

[1] C. E. Brennen, “An Introduction to Cavitation Fundamentals,” in *Cavitation: Turbo-machinery & Medical Applications*, Coventry, UK, 2011.

[2] C. E. Brennen, “Phase Change, Nucleation, and Cavitation,” in *Cavitation and Bubble Dynamics*, Pasadena, USA, Cambridge University Press, 1995, pp. 1-29.

[3] M. Zamoum and M. Kessal, "Analysis of cavitating flow through a venturi," *Scientific Research and Essays,* vol. 10 (11), pp. 367-375, 2015.

[4] J. D. Bressan, M. A. Klemz and G. Bazanini, “Cavitation Erosion Damage of Metallic Materials in Rotating Disk Testing,” in *Second International Brazilian Conference on Tribology - Tribo BR*, Foz do Iguacu, Brazil, 2014.

[5] V. H. Arakeri, “Contributions to some cavitation problems in turbomachinery,” *Sādhanā,* vol. 24, no. 6, pp. 453-483, 1999.

[6] M. Müller, Dynamic behaviour of cavitation bubbles generated by laser, Liberec, Czech Republic: Technical University of Liberec, 2008.

[7] J. W. S. Rayleigh, “On the pressure developed in a liquid during the collapse of a spherical cavity,” *The London, Edinburgh, and Dublin Philosophical Magazine and Journal of Science,* vol. 8, pp. 94-98, 1917.

[8] J.-P. Franc and J.-M. Michel, Fundamentals of Cavitation, Kluwer Academic Publishers, 2005.

[9] C. E. Brennen, “Spherical Bubble Dynamics,” in *Cavitation and Bubble Dynamics*, Pasadena, USA, Cambridge University Press, 2014, pp. 30-58.

[10] C. E. Brennen, “Cavitation Bubble Collapse,” in *Cavitation and Bubble Dynamics*, Pasadena, USA, Cambridge University Press, 2014, pp. 59-88.

[11] K.-H. Kim, G. Chahine, J.-P. Franc and A. Karimi, Advanced Experimental and Numerical Techniques for Cavitation Erosion Prediction, Springer, 2014.

[12] P. Jarman, “Sonoluminescence: A Discussion,” *The Journal of the Acoustical Society of America,* vol. 32, no. 11, pp. 1459-1462, 1960.

[13] C. Herring, “Theory of the pulsations of the gas bubble produced by an underwater explosion,” Columbia University, Division of National Defense Research, New York City, USA, 1941.

[14] L. Trilling, “The Collapse and Rebound of a Gas Bubble,” *Journal of Applied Physics,* vol. 23, pp. 14-17, 1952.

[15] F. R. GIlmore, "The growth or collapse of a spherical bubble in a viscous compressible liquid," California Institute of Technology, Pasadena, USA, 1952.

[16] K. Vokurka, “Comparison of Rayleigh's, Herring's, and Gilmore's Models of Gas Bubbles,” *Acta Acustica,* vol. 3, no. 59, pp. 214-219, 1986.

[17] W. Y. Tey, H. Allehossein, Z. Qin, K. M. Lee, H. S. Kang and K. Q. Lee, “On stability of time marching in numerical solutions of Rayleigh-Plesset equation for ultrasonic cavitation,” in *IOP Conference Series: Earth and Environmental Science (EES)*, Bangkok, Thailand, 2020.

[18] S. S. Chapra, "Runge-Kutta methods," in *Applied Numerical Methods with MATLAB*, Massachusetts, USA, McGraw-Hill, 2012, pp. 567-571.

[19] M. Brdička, L. Samek a O. Taraba, „Kavitace - Diagnostika a technické využití,“ v *Kavitace - Diagnostika a technické využití*, Prague, Czech Republic, Nakladatelství technické literatury, 1981, p. 92.

[20] S. Zhu, F. H. Cocks, G. M. Preminger and P. Zhong, “The role of stress waves and cavitation in stone comminution in shock wave lithotripsy,” *Ultrasound in Medicine & Biology,* vol. 28 (5), pp. 661-671, 2002.

[21] G. Sinibaldi, A. Occhicone, F. A. Pereira, D. Caprini, L. Marino, F. Michelotti and C. M. Casciola, "Laser induced cavitation: Plasma generation and breakdown shockwave," *Physics of Fluids,* vol. 31, no. 10, 2019.

[22] D. Jašíková, M. Müller, M. Kotek and V. Kopecký, "The study of single cavitation bubble generated with LIB technique and its force impact on the solid wall," in *Recent Advances in Civil Engineering and Mechanics*, Florence, Italy, 2014.

[23] B. H. T. Goh, Y. D. A. Oh, E. Klaseboer, S. W. Ohl and B. C. Khoo, "A low-voltage spark-discharge method for generation of consistent oscillating bubbles," *Review of Scientific Instruments,* vol. 84 (1), 2013.

[24] F. Avellan and P. Dupont, "Prediction of Cavitation Erosion: An Energy Approach," *Journal of Fluids Engineering,* vol. 120 (4), 1998.

[25] A. Vogel and S. Busch, "Shock wave emission and cavitation bubble generation by picosecond and nanosecond optical breakdown in water," *The Journal of the Acoustical Society of America,* vol. 100, pp. 148-165, 1996.

[26] E. Axdahl, "Britannica," [Online]. Available: https://www.britannica.com/science/cavitation. [Accessed 28 May 2021].

[27] S. C. Roy, "Doctoral dissertation: Modeling and analysis of material behavior during cavitation erosion," Université Grenoble Alpes, Grenoble, France, 2015.

APPENDIX A – Applying 4th order RK method to the system of equations

Procedure starts by the standard Rayleigh-Plesset equation, but disregarding surface tension *S* and liquid kinematic viscosity *v*:

$$R\frac{d\dot{R}}{dt}+\frac{3}{2}\left(\frac{dR}{dt}\right)^{2}=\frac{p_b(t)-p_\infty}{\rho} \qquad \text{A.1}$$

By dividing both sides of the equation A.1 by radius *R* we obtain:

$$\frac{d\dot{R}}{dt}+\frac{1}{R}\frac{3}{2}\left(\frac{dR}{dt}\right)^{2}+\frac{p_\infty-p_b(t)}{\rho} \qquad \text{A.2}$$

Since equation A.2 is a second order differential equation, in order for it to be solved it has to be transformed into a system of two first order ordinary differential equations (ODE):

$$\frac{dR}{dt}=z \qquad \text{A.3}$$

$$\frac{dz}{dt}=-\frac{1}{R}\frac{3}{2}z^{2}-\frac{1}{R}\left(\frac{p_\infty-p_b(t)}{\rho}\right) \qquad \text{A.4}$$

Applying fourth order Runge-Kutta method to the system of equations A.3 and A.4 is done firstly by specifying initial conditions $R\ (t=0) = 1.6 \times 10^{-5}\ m$ and $dR/dt\ (t=0) = 0$. Step size is $dt = 10^{-7}\ s$.

Coefficients k_0 through k_3, and l_0 through l_3 for the first time step are calculated as follows:

$$k_0 = dt \cdot \frac{dR}{dt}(t=0) \tag{A.5}$$

$$l_0 = dt \cdot \left[-\frac{1}{R(t=0)} \frac{3}{2} \left(\frac{dR}{dt}(t=0) \right)^2 - \frac{1}{R(t=0)} \left(\frac{p_\infty(t=0) - p_v - p_{g0} \left(\frac{R_0}{R(t=0)} \right)^{3k}}{\rho} \right) \right] \tag{A.6}$$

$$k_1 = dt \cdot \left[\frac{dR}{dt}(t=0) + \frac{l_0}{2} \right] \tag{A.7}$$

$$l_1 = dt \cdot \left[-\frac{1}{R(t=0) + \frac{k_0}{2}} \frac{3}{2} \left(\frac{dR}{dt}(t=0) + \frac{l_0}{2} \right)^2 - \frac{1}{R(t=0) + \frac{k_0}{2}} \left(\frac{p_\infty(t=0) - p_v - p_{g0} \left(\frac{R_0}{R(t=0) + \frac{k_0}{2}} \right)^{3k}}{\rho} \right) \right] \tag{A.8}$$

$$k_2 = dt \cdot \left[\frac{dR}{dt}(t=0) + \frac{l_1}{2} \right] \tag{A.9}$$

$$l_2 = dt \cdot \left[-\frac{1}{R(t=0) + \frac{k_1}{2}} \frac{3}{2} \left(\frac{dR}{dt}(t=0) + \frac{l_1}{2} \right)^2 - \frac{1}{R(t=0) + \frac{k_1}{2}} \left(\frac{p_\infty(t=0) - p_v - p_{g0} \left(\frac{R_0}{R(t=0) + \frac{k_1}{2}} \right)^{3k}}{\rho} \right) \right] \tag{A.10}$$

$$k_3 = dt \cdot \left[\frac{dR}{dt}(t=0) + l_2\right] \tag{A.11}$$

$$l_3 = dt \cdot \left[-\frac{1}{R(t=0)+k_2}\frac{3}{2}\left(\frac{dR}{dt}(t=0) + l_2\right)^2 - \frac{1}{R(t=0)+k_2}\left(\frac{p_\infty(t=0) - p_v - p_{g0}\left(\frac{R_0}{R(t=0)+k_2}\right)^{3k}}{\rho}\right)\right] \tag{A.12}$$

Once coefficients have been obtained, it is possible to calculate radius and velocity of the bubble in a given time step:

$$R\big((t=0)+dt\big) = R(t=0) + \frac{1}{6}\left(k_0 + \frac{k_1}{2} + \frac{k_2}{2} + k_3\right) \tag{A.13}$$

$$\frac{dR}{dt}\big((t=0)+dt\big) = \frac{dR}{dt}(t=0) + \frac{1}{6}\left(l_0 + \frac{l_1}{2} + \frac{l_2}{2} + l_3\right) \tag{A.14}$$

APPENDIX B – Bubble radii values obtained experimentally and by the model - comparison

Table B.1 Laser-induced bubble - comparison of experimental and model radii

Time [μs]	Experimental radius [mm]	Model radius [mm]
5.55	0.47	0.47
11.10	0.68	0.47
16.65	0.80	0.49
22.20	0.89	0.54
27.75	1.02	0.64
33.30	1.06	0.73
38.85	1.10	0.83
44.40	1.10	0.90
49.95	1.14	0.99
55.50	1.14	1.04
61.05	1.14	1.08
66.60	1.10	1.08
72.15	1.10	1.09
77.70	1.02	1.05
83.25	1.02	1.02
88.80	0.93	0.97
94.35	0.85	0.89
99.90	0.72	0.74
105.45	0.51	0.54
111.00	0.25	0.21
116.55	0.47	0.44
122.10	0.55	0.57
127.65	0.59	0.63
133.20	0.64	0.69
138.75	0.64	0.71
144.30	0.55	0.60
149.85	0.51	0.54
155.40	0.42	0.38

Table B.2 First spark-generated bubble – comparison of experimental and model radii

Time [ms]	Experimental radius [mm]	Model radius [mm]
0.10	0.24	0.24
0.20	1.67	0.76
0.30	2.71	1.74
0.40	3.39	2.69
0.50	3.88	3.51
0.60	4.24	4.10
0.70	4.46	4.44
0.80	4.55	4.55
0.90	4.58	4.59
1.00	4.53	4.66
1.10	4.27	4.61
1.20	3.96	4.53
1.30	3.41	4.09
1.40	2.47	3.06
1.50	0.99	1.24
1.60	1.70	2.13
1.70	1.75	2.21
1.80	1.55	1.98
1.90	1.24	1.62

Table B.3 Second spark-generated bubble – comparison of experimental and model radii

Time [ms]	Experimental radius [mm]	Model radius [mm]
0.10	0.26	0.26
0.20	1.21	0.56
0.30	1.95	1.29
0.40	2.38	1.89
0.50	2.50	2.26
0.60	2.53	2.45
0.70	2.43	2.41
0.80	2.11	2.11
0.90	1.40	1.40
1.00	1.24	1.28
1.10	1.39	1.50
1.20	1.15	1.31